AFWAL-TR-88-2141

SUPERIONICS

R. F. Wallis

University of California, Irvine

Department of Physics

Irvine, California 92717

March 1989

Final Report for Period April 85 to June 88

AERO PROPULSION LABORATORY

AIR FORCE WRIGHT AERONAUTICAL LABORATORIES

AIR FORCE SYSTEMS COMMAND

WRIGHT-PATTERSON AIR FORCE BASE, OHIO 45433-6563

NOTICE

When Government drawings, specifications, or other data are used for any purpose other than in connection with a definitely related Government procurement operation, the United States Government thereby incurs no responsibility nor any obligation whatsoever; and the fact that the government may have formulated, furnished, or in any way supplied the said drawings, specifications, or other data, is not to be regarded by implication or otherwise as in any manner licensing the holder or any other person or corporation, or conveying any rights or permission to manufacture use, or sell any patented invention that may in any way be related thereto.

This report is releasable to the National Technical Information Service (NTIS). At NTIS, it will be available to the general public, including foreign nations.

This technical report has been reviewed and is approved for publication.

Stephen P. Vukson

STEPHEN P. VUKSON
Project Engineer

B. L. McFADDEN, Chief
Power Technology Branch
Aerospace Power Division
Aero Propulsion and Power Laboratory

FOR THE COMMANDER

[illegible]
Aerospace Power Division
Aero Propulsion & Power Laboratory

If your address has changed, if you wish to be removed from our mailing list, or if the addressee is no longer employed by your organization please notify AFWAL/POOS-2 W-PAFB, OH 45433-6563 to help us maintain a current mailing list.

Copies of this report should not be returned unless is required by security considerations, contractual obligations, or notice on a specific document.

REPORT DOCUMENTATION PAGE

1a. REPORT SECURITY CLASSIFICATION: Unclassified	1b. RESTRICTIVE MARKINGS
2a. SECURITY CLASSIFICATION AUTHORITY	3. DISTRIBUTION/AVAILABILITY OF REPORT: Approval for public release; distribution is unlimited.
2b. DECLASSIFICATION/DOWNGRADING SCHEDULE	
4. PERFORMING ORGANIZATION REPORT NUMBER(S)	5. MONITORING ORGANIZATION REPORT NUMBER(S): AFWAL-TR-88-2141
6a. NAME OF PERFORMING ORGANIZATION: University of California, Irvine; 6b. OFFICE SYMBOL (If applicable)	7a. NAME OF MONITORING ORGANIZATION: Air Force Wright Aeronautical Laboratories Aero Propulsion Laboratory (AFWAL/POOS-2)
6c. ADDRESS (City, State and ZIP Code): Irvine, California 92717	7b. ADDRESS (City, State and ZIP Code): WPAFB, OH 45433-6563
8a. NAME OF FUNDING/SPONSORING ORGANIZATION: Defense Advanced Research Projects Agency; 8b. OFFICE SYMBOL (If applicable): DSO	9. PROCUREMENT INSTRUMENT IDENTIFICATION NUMBER: F33615-85-K-2501
8c. ADDRESS (City, State and ZIP Code): Arlington, VA 22209	10. SOURCE OF FUNDING NOS.

PROGRAM ELEMENT NO.	PROJECT NO.	TASK NO.	WORK UNIT NO.
62712E 62702E	3145	22	07

11. TITLE (Include Security Classification): Superionics	
12. PERSONAL AUTHOR(S): R. F. Wallis	
13a. TYPE OF REPORT: Final	13b. TIME COVERED: FROM 1 Apr 85 TO 30 Jun 88
14. DATE OF REPORT (Yr., Mo., Day): 1989 March 8	15. PAGE COUNT: 82
16. SUPPLEMENTARY NOTATION	

17. COSATI CODES		
FIELD	GROUP	SUB. GR.
20	12	

18. SUBJECT TERMS (Continue on reverse if necessary and identify by block number)
Solid-State Battery
Fast Ion Conductor
Intercalation

19. ABSTRACT (Continue on reverse if necessary and identify by block number)

The correlation between the infrared and Raman spectra of lithium borate glasses and their structure has been investigated. The results are consistent with the increasing incorporation of tetrahedrally coordinated boron into the boroxol rings with increasing Li_2O content. The spectra reveal the onset of crystallization as the annealing temperature increases. The variation of the ionic conductivity with temperature and composition is shown to be well described by a weak electrolyte theory. The conductivity increases by an order of magnitude when the fractional content of Li_2SO_4 increases from 0.00 to 0.15. A tight binding method has been used to calculate the energy bands of InSe and the activation energy for motion of Li^+ in the Van der Waals gap of InSe. The increase in resistance of a lithium borate glass sample when the Li^+ ions are required to flow into the Van der Waals gaps of a contiguous InSe sample has been investigated.

20. DISTRIBUTION/AVAILABILITY OF ABSTRACT: UNCLASSIFIED/UNLIMITED ☒ SAME AS RPT. ☐ OTIC USERS ☐	21. ABSTRACT SECURITY CLASSIFICATION: Unclassified

22a. NAME OF RESPONSIBLE INDIVIDUAL	22b. TELEPHONE NUMBER (Include Area Code)	22c. OFFICE SYMBOL
Stephen P. Vukson	513-225-5461	AFWAL/POOS-2

TABLE OF CONTENTS

LIST OF FIGURES

LIST OF TABLES

1. FAST ION CONDUCTION IN BORATE GLASSES B_2O_3-xLi_2O-yLi_2SO_4

1.1. Structure of borate glasses

1.1.1 Introduction

Fast ion conducting glasses are generally boron oxide or boron sulfur glasses doped with mobile ions such as Li^+, for example. Fast ion conducting glasses can be regarded as a solution of a dopant salt such as Li_2SO_4 in a matrix composed of the glass forming materials such as B_2O_3 and its modifier Li_2O. Thus, a glass such as B_2O_3-xLi_2O-yLi_2SO_4 can be considered as a solution where Li_2SO_4 is the solute and B_2O_3-Li_2O is the solvent.

Investigating the molecular vibrations of the different components by Raman and infrared spectroscopies gives the possibility of performing a structural analysis and eventually of building up an overall representation of the glass structure.

We shall examine first the evidence for the existence of the different building blocks and then we shall concentrate on the possibility of inducing structural changes by varying external physical parameters such as the temperature, for example.

1.1.2. Structure of the glass former B_2O_3

The borate glasses v-B_2O_3 are generally good ionic and electronic insulators. There are strong arguments, from spectroscopic data, that the structure contains mainly rings whose breathing mode is Raman active and shows up as a sharp peak at 806 cm^{-1}. The existence of such a sharp structure should be surprising for a glass where one should expect to observe only very broad bands. The reason is that the sharp structures are due to highly regular hexagonal rings of bonds connected into a

more disordered network. It is supposed that the vibrational mode, at 806 cm^{-1}, of these rings is decoupled from the general network and consequently is strongly localized. A condition for vibrational decoupling of the appropriate ring mode from the surrounding network has been derived[1]. This decoupling is accomplished by a near cancellation of central and noncentral forces within the ring acting on the high-coordination B atoms that connect to the network. Therefore the connecting atoms do not move during the ring vibration, and this explains the absence of a mode isotope shift when isotopic substitution is carried out on the connecting B atoms. A representation of the structural configuration of v-B_2O_3 is a given in Figure 1.

1.1.3. Effect of the modifier Li_2O

The addition of Li_2O to the B_2O_3 modifies the structure of the glass. As the oxygen content increases in the glass with increasing concentration of Li_2O, an increasing number of B atoms becomes tetrahedrally coordinated. The maximum number of boron atoms with coordination number four (BO_4) occurs for a concentration of x of Li_2O of the order of 40%[2]. The addition of the modifier, Li_2O, into the glass B_2O_3 leads to the dissociation of the metal oxide with the formation of a tetrahedral radical and metallic ions

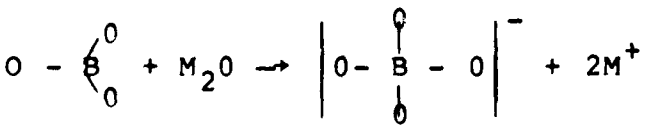

A BO_4 unit can be introduced into a boroxol ring in various ways[3].

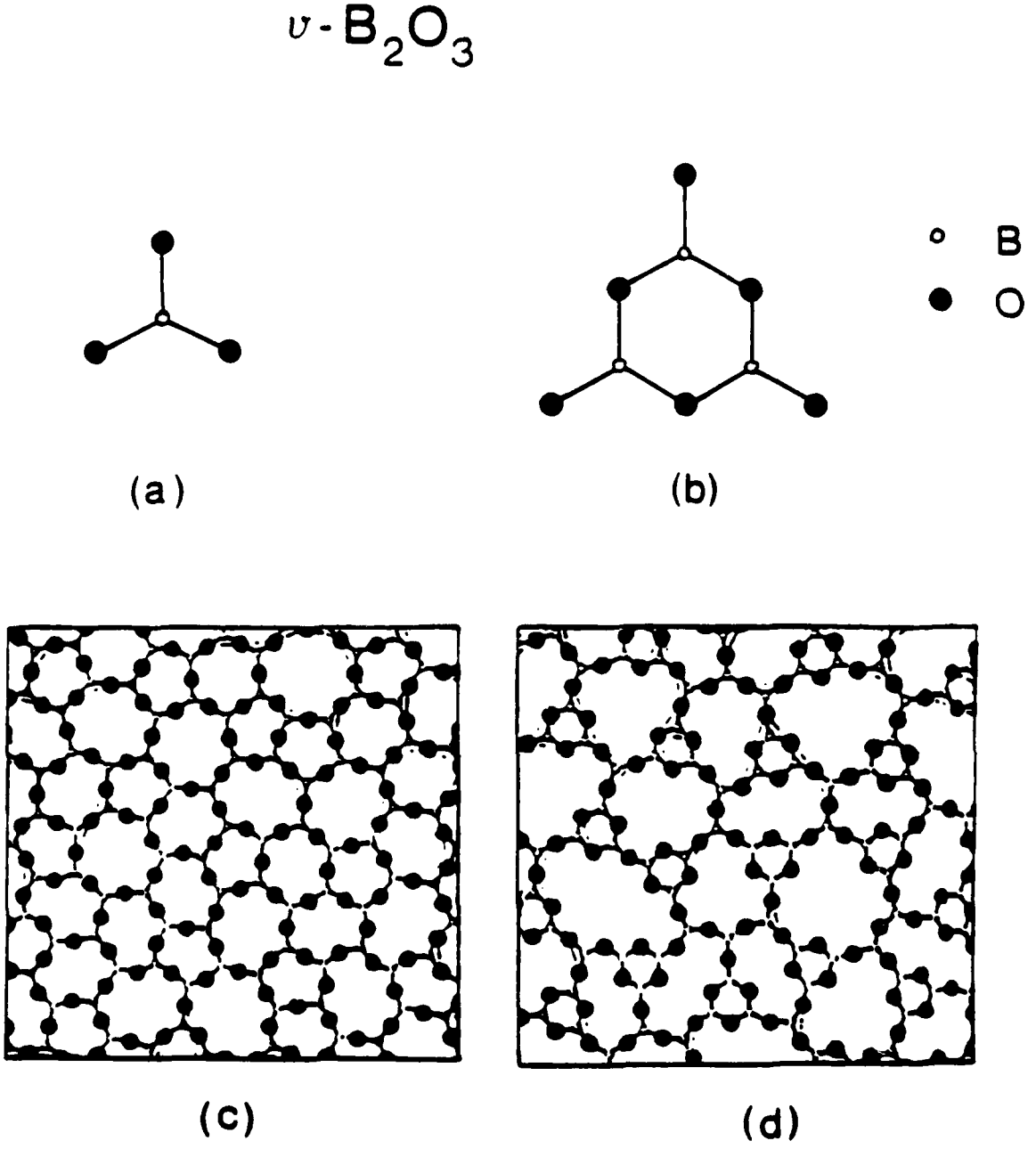

Figure 1. Structure of B_2O_3: (a) triangle of BO_3; (b) planar ring of boroxol, stabilized by delocalized π bonds; (c) representation of a random network; (d) structure of B_2O_3 with rings of boroxol.

The simplest hypothesis is to imagine that the boroxol rings are progressively replaced by triborate groups (Figure 2).

From conductivity measurements[4] one can deduce that B_2O_3-xLi_2O is a purely ionic conductor with Li^+ as the mobile species.

Increasing the Li_2O concentration x causes the frequency of the breathing mode attributed to the B_3O_6 ring with BO_4 groups to decrease, $\omega \simeq 770\ cm^{-1}$, and the asymmetry of the band to increase toward the lower energies as shown in Figure 3. This effect seems to be moderated by the addition of Li_2SO_4.

These changes of frequencies and half-width may be due to the appearance in the matrix conformation of more complex configurations in the B_3O_6 rings such as tetraborate and pentaborate groups shown in Figure 4.

1.1.4. Effect of the dopant Li_2SO_4

The addition of Li_2SO_4 up to the concentration used in the experiments, y = 0.42, does not seem to significantly affect the vibrational frequencies of the borate matrix. The matrix is formed by B_3O_6 rings containing one or more B atoms of coordination number 4, whose characteristic frequency is 780 cm^{-1}. In the case of borate glasses with x = 0.5 the rings are probably mainly triborates but the existence of diborates and ditriborates cannot be excluded.

The presence of the dopant Li_2SO_4 in lithium borate glasses can be easily identified by Raman spectroscopy.

The Raman spectrum of B_2O_3-0.7Li_2O-0.42Li_2SO_4 shown in Figure 5 is clearly the superposition of the Raman spectrum of

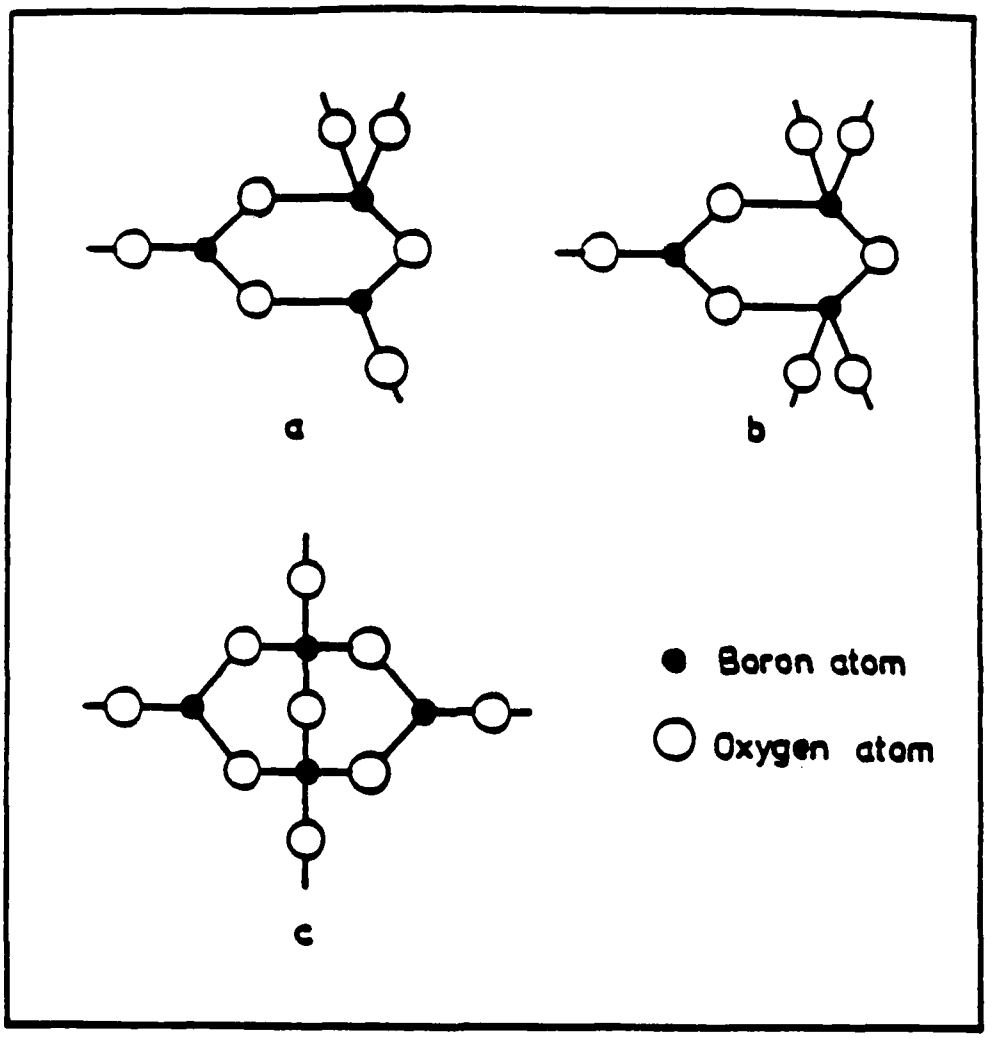

Figure 2. Some of the structural groups appearing in the alkali borates: (a) triborate; b) ditriborate; c) diborate.

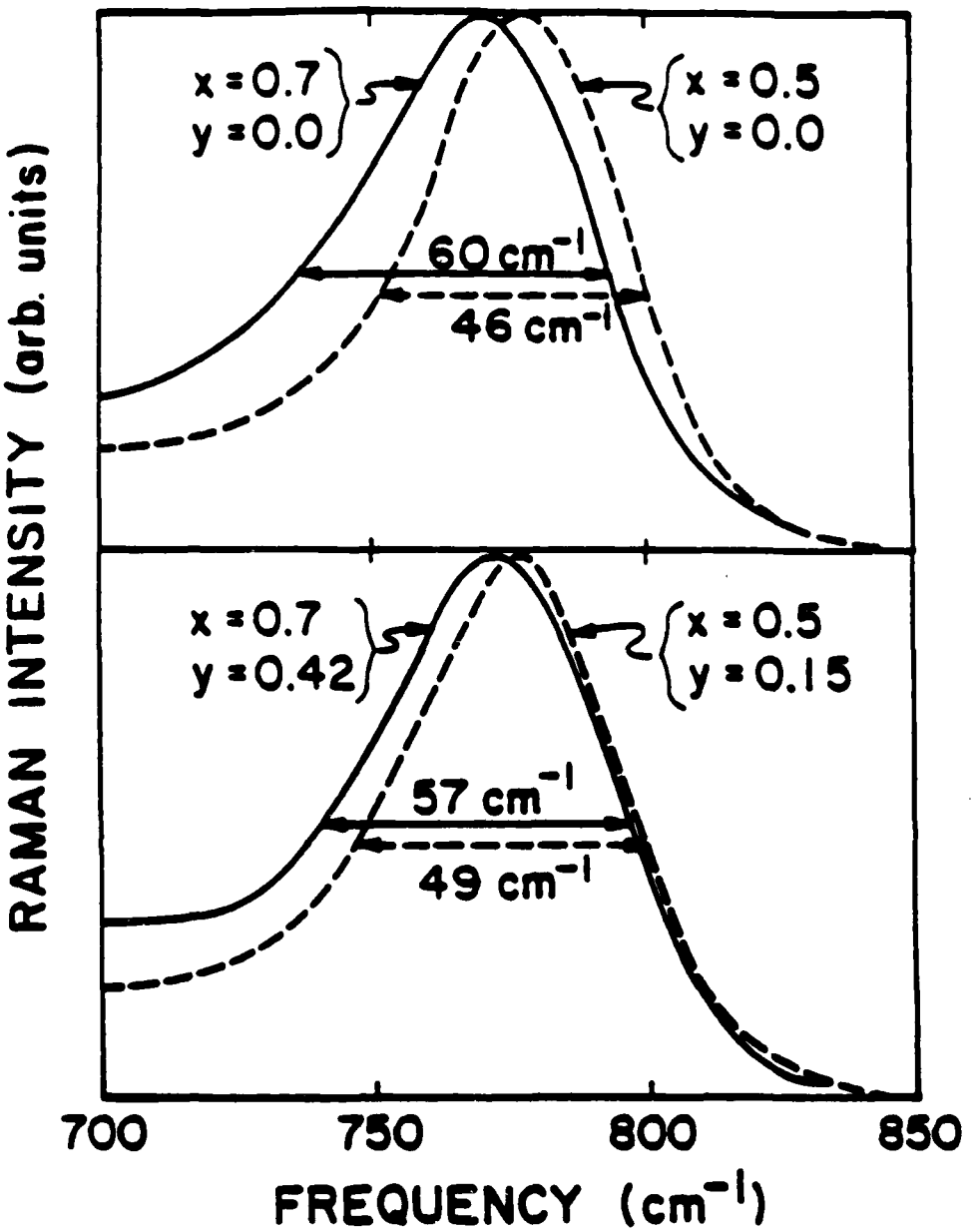

Figure 3. Raman peaks corresponding to the breathing symmetrical mode of the B_3O_6 cycles as a function of the Li concentration.

A: B_2O_3-0.5Li_2O and B_2O_3-0.7Li_2O

B: B_2O_3-0.5Li_2O-0.15Li_2SO_4 and B_2O_3-0.7Li_2O-0.42Li_2SO_4

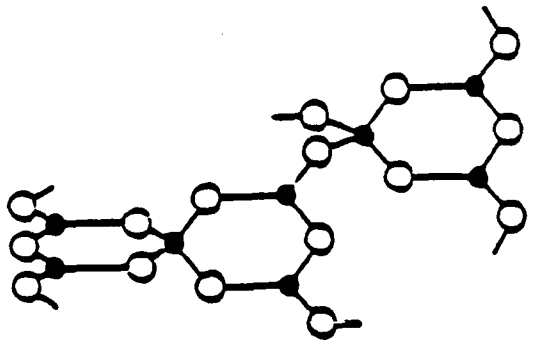

tetraborate group

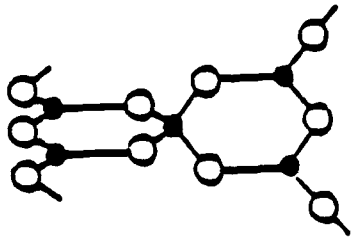

pentaborate group

Figure 4. Structural group appearing in the alkali borates: tetraborates and pentaborates.

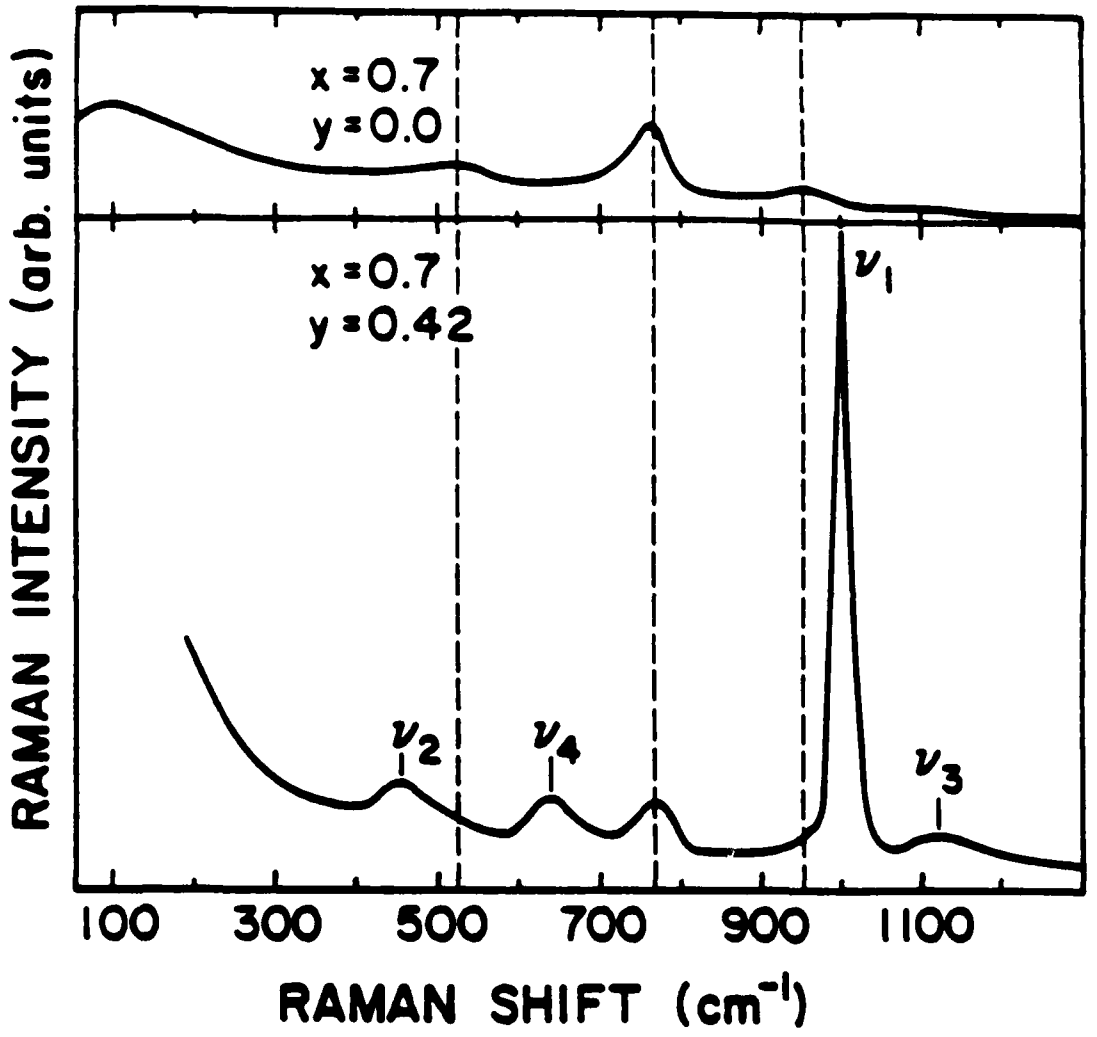

Figure 5. Raman spectra for B_2O_3-0.7Li_2O-y-Li_2SO_4 for y=0; 0.42 at room temperature without annealing. Laser beam at 514.5 nm, resolution 2 cm^{-1}.

the matrix B_2O_3-0.7Li_2O and that of the solute Li_2SO_4. Peaks such as ν_1, ν_2, ν_3 and ν_4 are those of the characteristic vibrational modes of SO_4^{--}. The sharp peak shown on top of Figure 1 is that of the matrix B_2O_3-0.7Li_2O.

1.1.5. Temperature annealing, glass crystalline transition in borate glasses

Progressive thermal annealing[5] of borate glasses leads to the crystalline phase of B_2O_3-x$Li_{22}O$-yLi_2SO_4 through successive configurational transformations of the matrix. The experiments[6] are conducted as follows: the samples are submitted by slow heating to a given annealing temperature T_a and held at that temperature for one hour; then, are rapidly quenched to room temperature. After this treatment, the Raman spectra are taken at room temperature. We will examine successively the different parts of these spectra.

1.1.5.1. The breathing mode $\nu_1(A_1)$ of SO_4^{--}

When the annealing temperature increases progressively from 470°C to 550°C the characteristic peak for the SO_4^{--} mode situated initially at 1006 cm^{-1} first decreases in intensity and then disappears. A new peak then appears at 1016 cm^{-1} which has still the frequency of the SO_4^{--} breathing mode but now in the crystalline phase of Li_2SO_4. This transformation can be followed closely in Figure 6.

The temperature at which the crystallization of Li_2SO_4 occurs, signalled by the appearance of the peak at higher frequencies near 1016 to 1020 cm^{-1}, depends on the borate

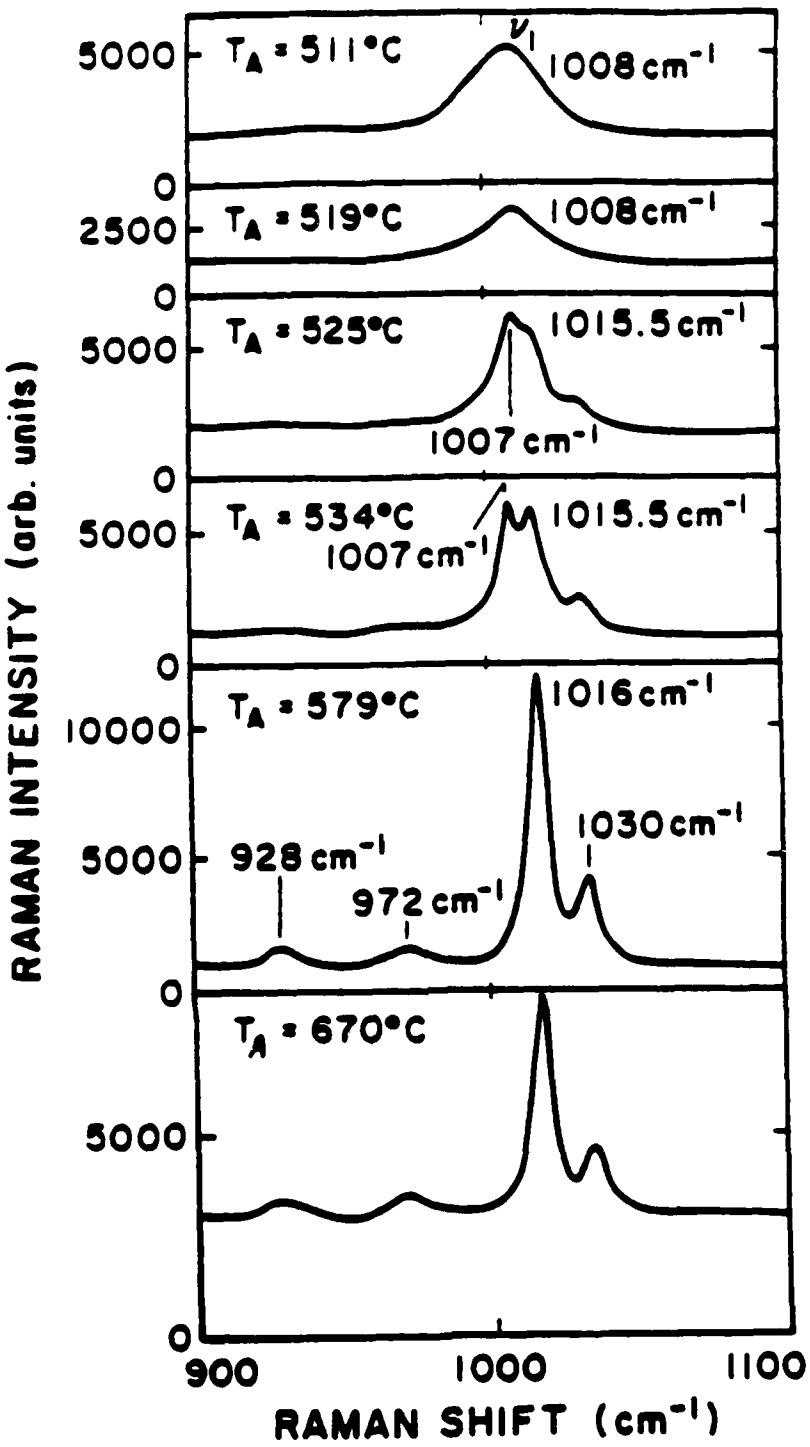

Figure 6. Raman spectra for different annealing temperatures of B_2O_3-0.5Li_2O-0.15Li_2SO_4 centered at the mode $\nu_1(A_1)$. Spectra taken at room temperature with a laser beam at 514.5 nm having a power of 250 mW and with an instrumental resolution of 2 cm^{-1}.

composition. For B_2O_3-0.5Li_2O-0.1Li_2SO_4 the new peak at 1016 cm^{-1} shows up at 516°C and is fully developed after the disappearance of the peak at 1006 cm^{-1} at 540°C. For B_2O_3-0.5Li_2O-0.15Li_2SO_4 the peak at 1016 cm^{-1} appears at 525°C and the 1008 cm^{-1} peak disappears completely at 579°C; whereas for B_2O_3-0.7Li_2O-0.42Li_2SO_4 the second peak is already clearly visible at 475°C and shows a frequency of 1020 cm^{-1}. The first peak initially situated at 1012 cm^{-1} disappears above 511°C. The remark to be made here is that the higher the concentration of Li_2O and Li_2SO_4, the lower the annealing temperature at which the Li_2SO_4 crystallites appear and the stiffer the SO_4^{--} ν_1 mode. The stiffening of the breathing mode probably occurs through electrostatic interactions. The higher the ion concentration is, the stronger the repulsive force is among the SO_4^{--} ions. This is an effect equivalent to increasing pressure and therefore stiffening the symmetric mode frequencies.

1.1.5.2. The breathing mode of the B_3O_5 ring

In the glasses with the diborate matrix B_2O_3-0.2Li_2O above an annealing temperature of 510°C one observes the appearance of a new peak at 725 cm^{-1}, as shown in Figure 7.

For annealing temperatures above 560°C the observed spectrum is identical so that of crystalline diborate B_2O_3-0.5Li_2O[7]. The crystallization of the borate matrix into the forms of diborate is also accompanied by the appearance of a peak at 1030 cm^{-1} at 525°C as evidenced by spectra shown in Figure 6.

One should notice also the appearance in the crystalline phase of a weak peak situated at 772-774 cm^{-1} attributed to the

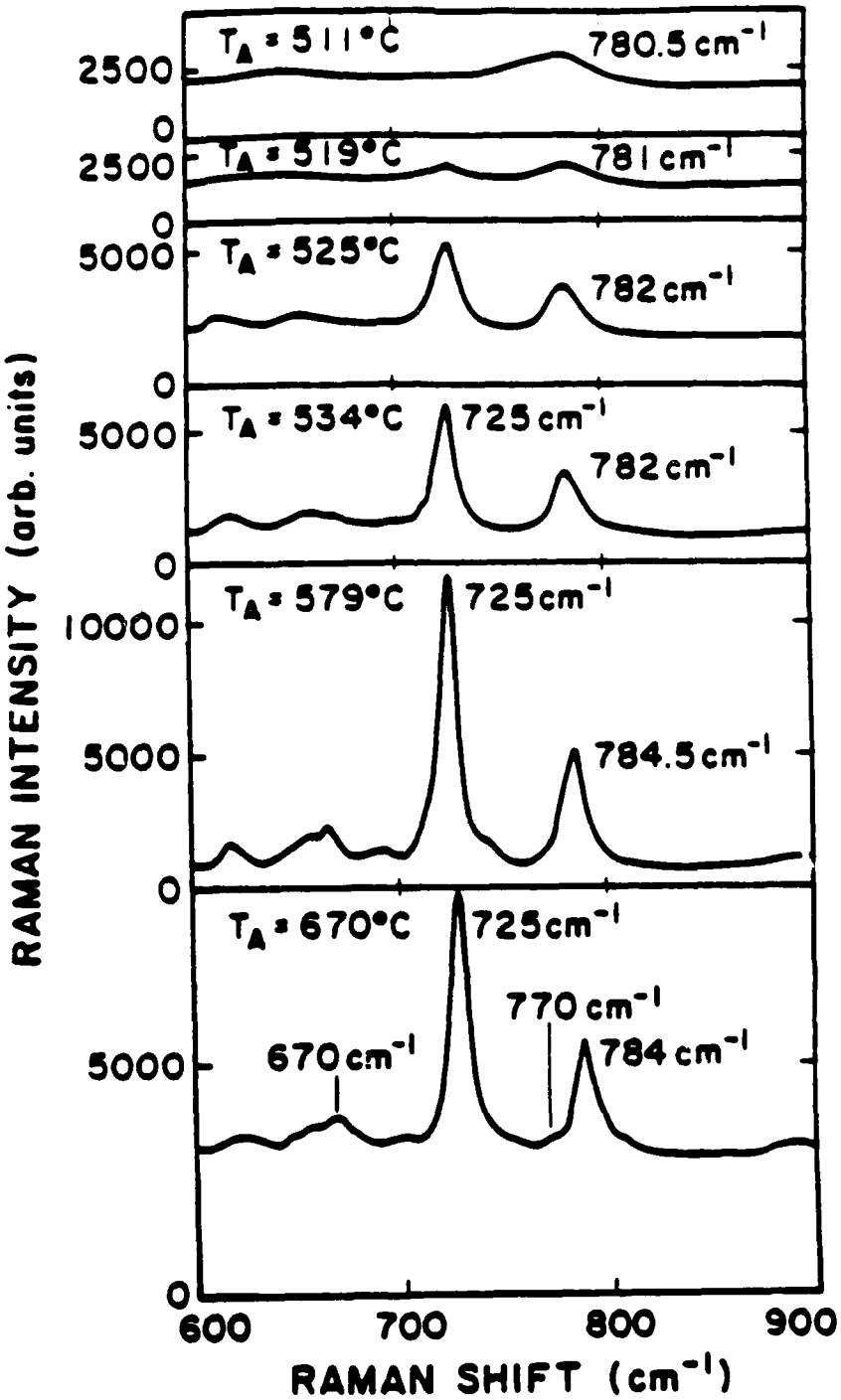

Figure 7. Raman spectra of B_2O_3-0.5Li_2O-0.15Li_2SO_4 for different annealing temperatures focussed at the frequency region of the characteristic modes of crystalline diborate. Spectra taken with a laser beam of 514.5 nm and power of 250 mW. The instrumental resolution is 2 cm^{-1}.

formation of some ditriborate groups[8].

Depending on the glass matrix composition, the crystallization of the matrix may occur at a lower temperature than the dopant salt if $x < 0.5$ and after the crystallization of the salt if $x > 0.5$. The respective crystallization temperatures for different glass compositions are listed in Table 1.[6] T_b and T_s are the crystallization temperatures of the borate glass matrix and dopant salt, respectively.

TABLE 1

CRYSTALLIZATION TEMPERATURES FOR DOPED BORATE GLASSES

B_2O_3-xLi_2O-yLi_2SO_4		T_b (° C)	T_s (° C)
x	y		
0.5	0.05	514	529
0.5	0.10	516	536
0.5	0.15	519	525
0.7	0.2	525	478
0.7	0.4	522	500
0.7	0.6	526	518

1.2. Ionic conductivity in lithium borate glasses

1.2.1. Introduction

The electrical properties of B_2O_3-xLi_2O-yLi_2SO_4 have been studied by the method of complex impedance in the range of 10^{-3} - 10^{-4} Hz. Gold evaporated electrodes have been used and the measurements performed in the temperature range between 20 and 400°C. Determination of the transport number by the method of blocking electrodes[9] confirms that the material is an electronic insulator.

Figure 8 shows the variation of the conductivity as a function of the temperature[10]. When x and y are relatively high the conductivity is good, $\sigma = 2.10^{-2}\ \Omega^{-1}\ cm^{-1}$ at 300°C, and the activation energy is of the order of the 0.58 eV.

Figure 9 gives the evolution of the conductivity at 300°C as a function of the Li_2SO_4 concentration y for the different content of Li_2O, x. For a given x the conductivity increases with increasing y. The conductivity rise is very rapid for $x < 0.43$ and becomes much slower for $x > 0.71$. A saturation occurs which corresponds to the non-dissociation of Li_2SO_4 and its crystallization which limits the vitreous domain. The vitreous domain as a function of the concentration for B_2O_3-xLi_2O-yLi_2SO_4 is shown in Figure 10.

The results on ionic conductivity reported here are obtained by complex impedance measurements in the frequency range 5 Hz to 13 MHz with a Hewlett-Packard 4192 ALF impedance analyzer. The samples used are rectangular slabs of dimensions 4x2.5x1 mm. Platinum electrodes of circular configuration are vapor deposited

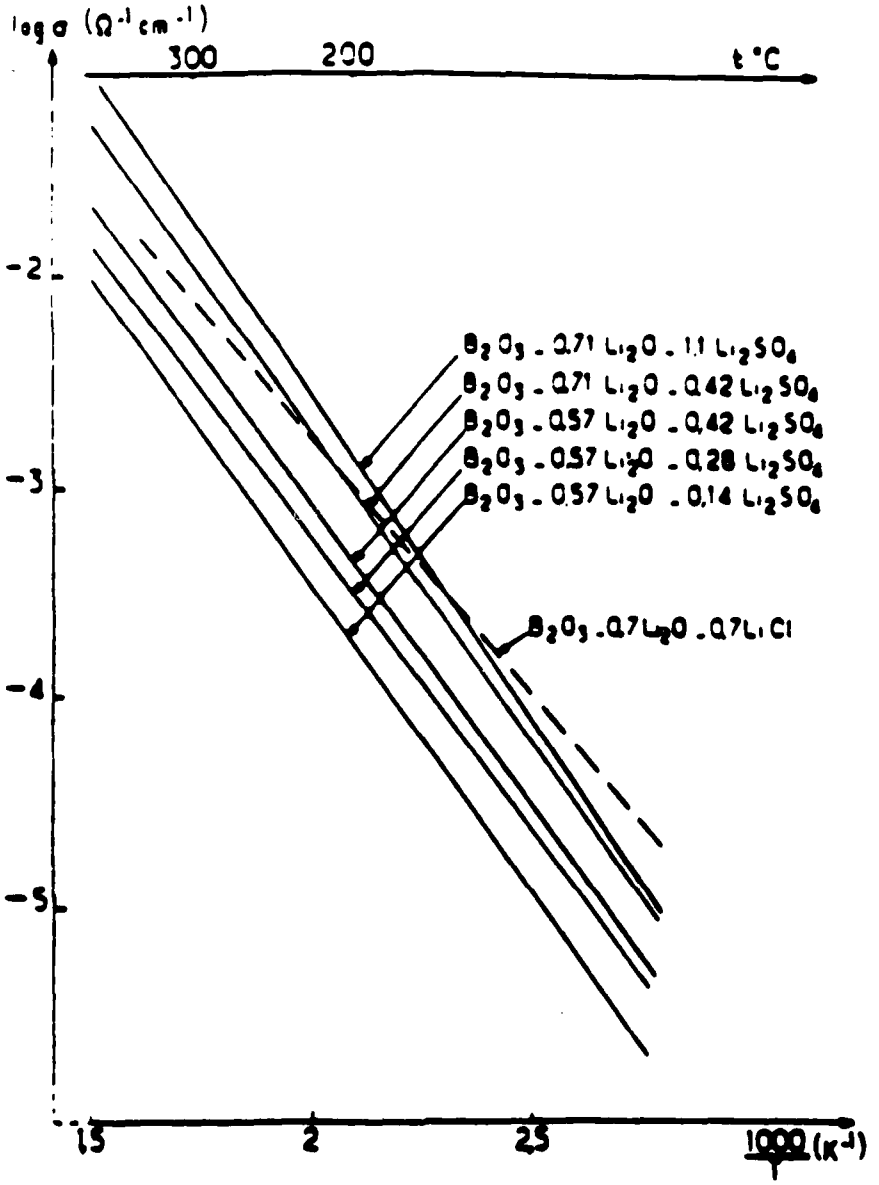

Figure 8. Variation of the Li^+ conductivity as a function of the reciprocal temperature for the borate glasses B_2O_3-xLi_2O-yLi_2SO_4 for different concentrations x of Li_2O and y of Li_2SO_4 according to reference 10. The same variation for B_2O_3-0.7 Li_2O-0.7 LiCl is represented by the broken line (A. Levasseur, J. C. Brethous, J. M. Réau and P. Hagenmuller, Mat. Res. Bull. 1979).

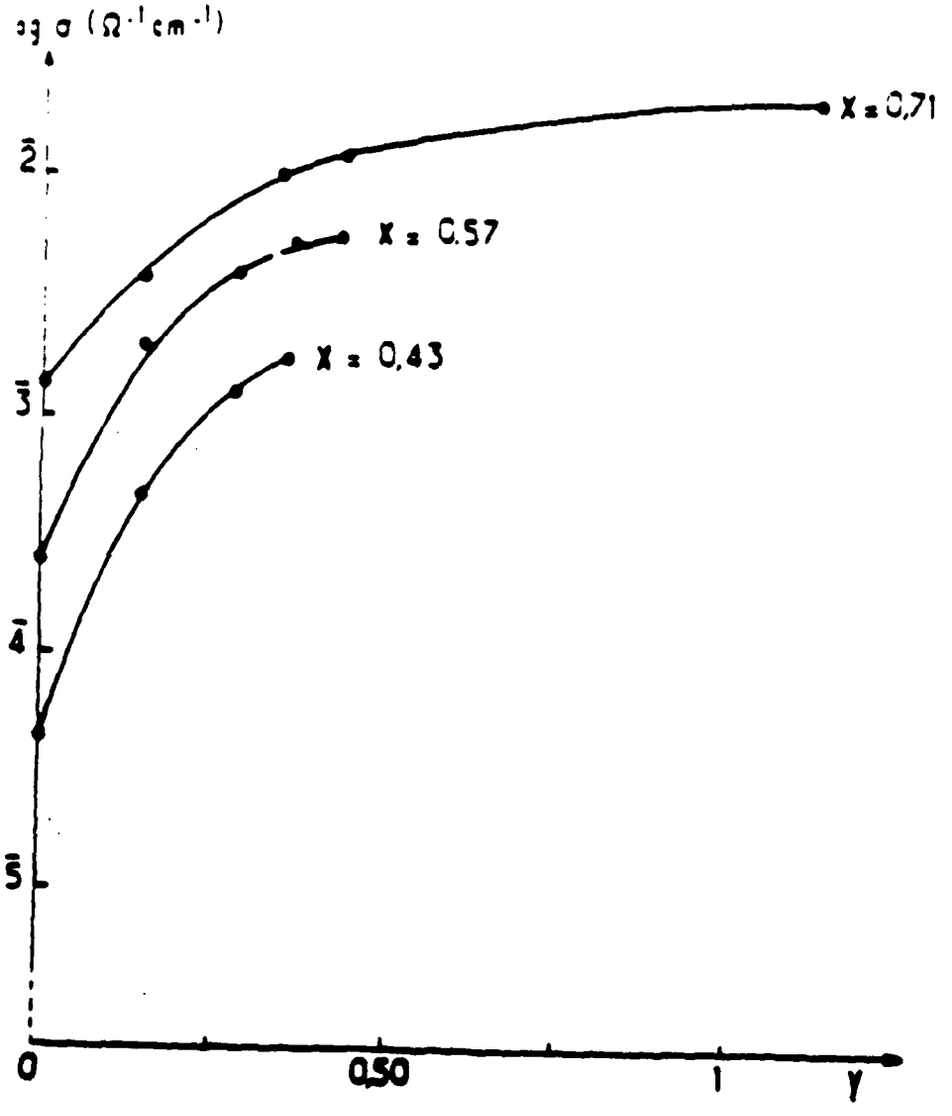

Figure 9. Variation of the Li^+ conductivity at 300°C in B_2O_3-xLi_2O-yLi_2SO_4 as a function of the Li_2SO_4 concentration y, for different Li_2O concentrations x according to reference 10.

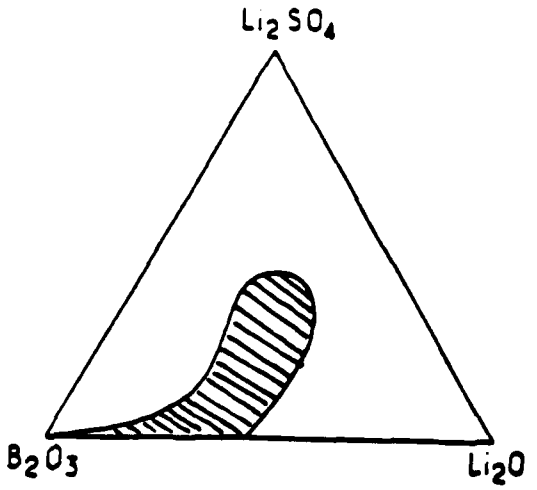

Figure 10. The vitreous domain for the system $B_2O_3Li_2O$-Li_2SO_4 according to reference 10.

on the two sides of the slab as shown in Figure 11. The applied voltage along the z direction is 500 mV.

1.2.2 Transport properties of B_2O_3-0.5Li_2O-yLi_2SO_4

The logarithm of the conductivity as a function of the reciprocal temperature for the different samples investigated is plotted in Figure 12. At the lower temperature side the conductivity follows the law

$$\sigma = \frac{\sigma_o}{T} \exp\left(-\frac{E_a}{kT}\right) \quad .$$

The deviations from this law observed at high temperature may be due to the difficulty of having a correct reading of the temperature at high temperatures.

The best conductivity measured is that of the samples with a Li_2SO_4 concentration of y = 0.15: $\sigma_{max} \sim 10^{-2}\ \Omega^{-1}\ cm^{-1}$ at 300°C. The activation energy for this sample is E_a = 0.6 eV.

1.2.3. Theoretical Analysis

1.2.3.1. Introduction

In the system that we are dealing with, a salt such as Li_2SO_4 is dissolved in a solid matrix consisting of a lithium borate glass. The salt dissociates giving Li^+ ions and $LiSO_4^-$ ions. The Li^+ ions are highly mobile and significantly increase the electrical conductivity of the system. The situation is quite analogous to an electrolytic solution where a salt is dissolved in a liquid solvent such as water. There is one significant difference, however, and that is that water has a dielectric constant of ~ 80 whereas borate glasses have a

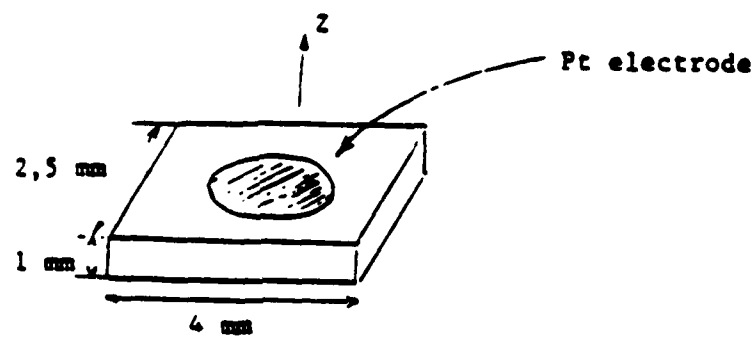

Figure 11. Sample configuration for the complex impedance measurements on B_2O_3-xLi_2O-yLi_2SO_4 showing the position of the platinum electrodes.

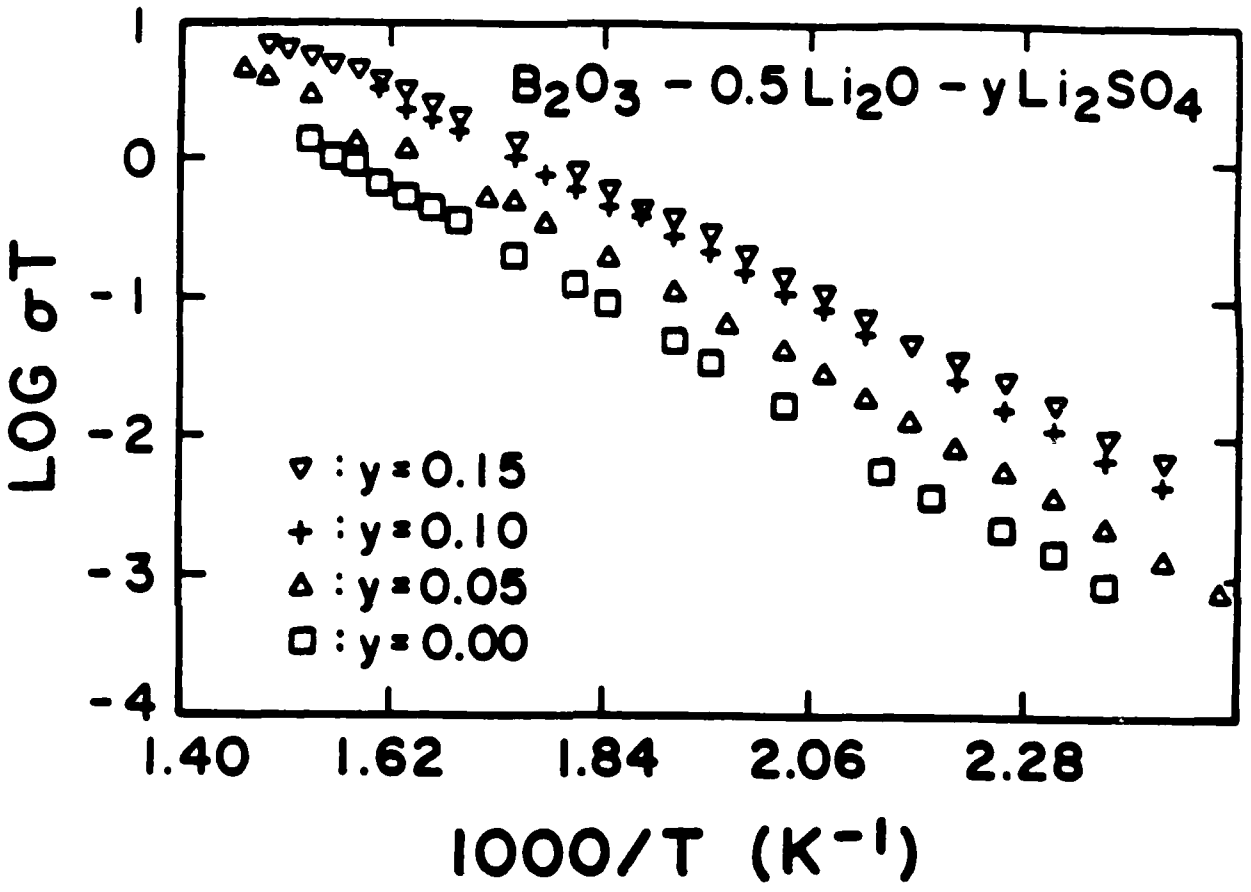

Figure 12. Variation of log σT as a function of the reciprocal absolute temperature for different concentrations y of Li_2SO_4 in B_2O_3-0.5 Li_2O-yLi_2SO_4.

dielectric constant of ~ 6. This means that at room temperature a typical salt such as Li_2SO_4 will be nearly fully dissociated in aqueous solution but will be only weakly dissociated in the borate glass. Furthermore, in the latter case, the concentration of lithium ions will increase rapidly as the temperature is increased above room temperature. Consequently, the electrical conductivity of the doped borate glasses should increase rapidly with increasing temperature, as seen in the experimental data discussed in Section 1.2 of this report. In the following sections, we shall develop a theory for the temperature dependence of the free lithium ion concentration and derive an expression for the activation energy characterizing the conductivity.

1.2.3.2. Calculation of mobile Li^+ ion concentration

Consider an ensemble of Li_2SO_4 molecules dispersed in the borate glass that is assumed to be a continuous medium. If we regard the molecules as isolated and assume that only one Li^+ ion can be ionized per molecule (these assumptions being valid in the low concentration limit at temperatures which are not too high) the energy of an Li^+ ion is given by

$$E(p,r) = \frac{p^2}{2M} + V(r) \qquad (1)$$

where V(r) is the Coulomb potential energy of the Li^+ ion in the field of the $LiSO_4^-$ given by

$$V(r) = -\frac{e^2}{\varepsilon r} \qquad (2)$$

p is the momentum of the Li^+ ion, r is its distance from the negative ion, M is the ion mass and ε is the static dielectric constant of the glass. The number of ions with energy E is given by the Boltzmann distribution

$$n(E) = A \exp \{ - \frac{E(p,r)}{k_B T} \} \tag{3}$$

where T is the absolute temperature and A is a normalization constant determined by the total number N of ions according to the expression

$$N = A \int d^3p \int d^3r \exp \{ - \frac{E(p,r)}{k_B T} \} \tag{4}$$

We wish to calculate the number N_B of bound Li^+ ions and the number N_F of free Li^+ ions which are given by

$$N_B = A \int d^3p \int d^3r \exp \{ - \frac{E(p,r)}{k_B T} \} \tag{5}$$

for $(E,p,r)<0$ and

$$N_F = A \int d^3p \int d^3r \exp \{ - \frac{E(p,r)}{k_B T} \} \tag{6}$$

for $E(p,r)>0$.

From Eqs. (1) and (2) we can see that the conditions $E(p,r)<0$ and $E(p,r)>0$ correspond to $p^2/2M<e^2/\varepsilon r$ and $p^2/2M>e^2/\varepsilon r$ respectively. Introducing spherical coordinates in both the p and r spaces, we can carry out the integrals over the angle

variables and obtain the expression

$$N_B = 16\pi^{1/2}A(2\pi Mk_BT)^{3/2}\lambda^3\left[-\frac{1}{5}\left\{\left(\frac{R}{\lambda}\right)^{5/2} - \left(\frac{r_0}{\lambda}\right)^{5/2}\right\} + \frac{\pi^{1/2}}{4}\int_{\lambda/R}^{\lambda/r_0} y^{-4} \exp(y)\,\mathrm{Erf}(y^{1/2})\,dy\right] \tag{7}$$

where $\lambda = e^2/\varepsilon k_BT$, Erf(x) is the error function, r_0 is the distance of closest approach of an Li^+ ion to an $LiSO_4^-$ ion, and R is the upper limit on the r integration, the value of which will be discussed shortly.

We can evaluate the right-hand side of Eq. (6) in a similar fashion to obtain an expression for N_F. This gives

$$N_F = 16\pi^{1/2}A(2\pi Mk_BT)^{3/2}\lambda^3\left[\frac{1}{5}\left\{\left(\frac{R}{\lambda}\right)^{5/2} - \left(\frac{r_0}{\lambda}\right)^{5/2}\right\} + \frac{\pi^{1/2}}{4}\int_{\lambda/R}^{\lambda/r_0} y^{-4} \exp(y) \times \mathrm{Erfc}(y^{1/2})\,dy\right] \tag{8}$$

where Erfc(x) is the complement of the error function given by Erfc(x) = 1 - Erf(x). It can be shown quite easily from Eqs. (4), (7) and (8) that

$$N_B + N_F = N \tag{9}$$

We now turn to the discussion of the upper limit R and the lower limit r_0 of the r integration. Suppose that initially an Li^+ ion is close to a given $LiSO_4^-$ ion. As the Li^+ ion moves further away from the $LiSO_4^-$ ion it will eventually come closer to a second $LiSO_4^-$ ion and will then move predominantly under the influence of this second ion. The upper limit R should therefore be approximately given by $R = r_i/2$ where r_i is the mean nearest-neighbor distance between $LiSO_4^-$ ions. In our picture the concentrations of the free Li^+ ions and the $LiSO_4^-$ ions have the same value n_F in terms of which we can express r_i using the relation

$$r_i = n_F^{-1/3} \tag{10}$$

Our subsequent analysis of the experimental data will show that $n_F \approx 10^{19}$ cm^{-3} and so $r_i \approx 5.0 \times 10^{-7}$ cm.

The lower limit r_0 can be estimated from Pauling's values[11] for the S-O distance and the radii for O and Li^+. Adding these values gives the result $r_0 = 2.70$Å.

We also need to make an estimate of the quantity λ which appears in Eqs. (7) and (8). For the experimental temperatures of interest ($T \approx 600$K) and for $\varepsilon = 6.5$, a typical value for lithium borate glasses, we find that $\lambda \approx 4.3 \times 10^{-7}$ cm. It should be noted that λ and r_i are of the same order of magnitude and that they are an order of magnitude larger than r_0.

Using these appraisals, i.e., that $\lambda \approx r_i >> r_0$, we can make approximate evaluations of the integrals in Eqs. (7) and (8) to

obtain the results

$$N_B \approx 4\pi A(2\pi M k_B T)^{3/2}\lambda^3\left(\frac{r_0}{\lambda}\right)^4 \exp\left(\frac{\lambda}{r_0}\right) \tag{11}$$

and

$$N_F \simeq 4\pi A(2\pi M k_B T)^{3/2}\lambda^3 (r_i/2\lambda)^3/\pi^{1/2} \quad . \tag{12}$$

Eliminating A from Eqs. (11) and (12) and using Eq. (10) give the relation

$$N_F = N_B n_\lambda e^{-\lambda/r_o}/n_F \tag{13}$$

where

$$n_\lambda = \frac{\lambda}{8\pi^{1/2} r_o^4} \quad . \tag{14}$$

Dividing both sides of Eq. (13) by the volume V of the sample, we get

$$\frac{n_B}{n_F^2} = \frac{1}{n_\lambda} e^{\lambda/r_o} = K(T) \tag{15}$$

where $N_F = V_F/V$ and $n_B = N_B/V$. Equation (15) is simply the mass action law for the reaction

$$Li_2SO_4 \rightleftarrows Li^+ + LiSO_4^-$$

with K(T) the equilibrium constant.

At this point we must take into account the fact that the conductivity is non-zero when y = 0 due to a small concentration of free Li^+ ions arising from the dissociation of Li_2O. When y becomes different from zero, there will still be some concentration n'_F of free Li^+ ions from the Li_2O which must be included in the total free Li^+ ion concentration n_{FT}. We proceed by writing down expressions for the numbers of bound Li^+ ions N'_B and free Li^+ ions N'_F that are analogous to Eqs. (7) and (8). The results are

$$N'_B = 16\pi^{1/2}A'(2\pi Mk_BT)^{3/2}\lambda^3\{-(1/5)[(\frac{R}{\lambda})^{5/2}-(\frac{r'_o}{\lambda})^{5/2}] + (\pi^{1/2}/4)\int_{\lambda/R}^{\lambda/r'_o} y^{-4}e^y Erf(y^{1/2})dy\} \quad (16)$$

and

$$N'_F = 16\pi^{1/2}A'(2\pi Mk_BT)^{3/2}\lambda^3\{(1/5)[(\frac{R}{\lambda})^{5/2}-(\frac{r'_o}{\lambda})^{5/2}] + (\pi^{1/2}/4)\int_{\lambda/R}^{\lambda/r'_o} y^{-4}e^y Erfc(y^{1/2})dy\} \quad (17)$$

where r'_o is the distance of closest approach of a Li^+ ion to a LiO^- ion, A' is determined from the relation $N'_B + N'_F = N'$, and N' is the total concentration of Li^+ ions that can be ionized from Li_2O according to the reaction $Li_2O \rightarrow Li^+ + LiO^-$. From Pauling's radii[11] we obtain the value of 2.0Å for r'_o.

We can obtain an approximate expression for N'_F by using the

same procedure that led to Eq. (12). The quantity r_i is now to be related to the mean nearest neighbor separation between any pair of negative ions, either LiO^- or $LiSO_4^-$, and is taken to be

$$r_i = (n_F + n_F')^{-1/3} \quad . \tag{18}$$

Taking $R = r_i/2$ and using the appraisals $\lambda \approx r_i >> r_o'$, we find that

$$N_F' \approx 4\pi A' (2\pi M k_B T)^{3/2} (r_i/2)^3/\pi^{1/2} \quad . \tag{19}$$

The values of r_i given by Eq. (18) should also be used in Eq. (12).

We now proceed in a fashion analogous to that which led to Eq. (15). The mass action laws for the two reactions

$$Li_2SO_4 \rightleftarrows Li^+ + LiSO_4^-$$

$$Li_2O \rightleftarrows Li^+ + LiO^-$$

take the form

$$\frac{n_B}{n_{FT} n_o} = \frac{1}{n_\lambda} e^{\lambda/r_o} = K(T) \tag{20}$$

$$\frac{n_B'}{n_{FT} n_o'} = \frac{1}{n_\lambda'} e^{\lambda/r_o'} = K'(T) \tag{21}$$

where $n_{FT} = n_F + n_F'$, n_o is the concentration of $LiSO_4^-$ ions, n_o' is

the concentration of LiO^- ions, n'_B is the concentration of Li^+ ions bound to LiO^- ions, and

$$n'_\lambda = \frac{\lambda}{8\pi^{1/2}(r'_o)^4} \quad . \tag{22}$$

Let us introduce the quantities $n = n_o + n_B$ and $n' = n'_o + n'_B$ which represent, respectively, the total concentrations of Li_2SO_4 and Li_2O. If we eliminate n_B and n'_B from the expressions for n and n' using Eqs. (21) and (22) and rearrange the results, we get

$$n_o = \frac{n}{1+n_{FT}K(T)} \tag{23}$$

$$n'_o = \frac{n'}{1+n_{FT}K'(T)} \quad . \tag{24}$$

From conservation of lithium, we can write

$$n_{FT} = n_o + n'_o \quad , \tag{25}$$

and eliminating n_o and n'_o with the aid of Eqs. (24) and (25), we obtain

$$n_{FT} = \frac{n}{1+n_{FT}K(T)} + \frac{n'}{1+n_{FT}K'(T)} \quad . \tag{26}$$

Since we expect that the quantities n_{FT}/n and n_{FT}/n' are small, we can assume that $n_{FT}K(T) \gg 1$ and $n_{FT}K'(T) \gg 1$. Equation (26) then simplifies to

$$n_{FT}^2 = \frac{n}{K(T)} + \frac{n'}{K'(T)} \quad . \tag{27}$$

Substituting the expressions for K(T) and K'(T) from Eqs. (20) and (21) into Eq. (27), and taking the square root of both sides leads to the result

$$n_{FT} = [yn_\lambda n_T e^{-2E_{ad}/k_B T} + xn'_\lambda n_T e^{-2E'_{ad}/k_B T}]^{1/2} \tag{28}$$

where $x = n'/n_T$,

$$E_{ad} = \frac{e^2}{2\varepsilon r_o} \quad , \tag{29}$$

and

$$E'_{ad} = \frac{e^2}{2\varepsilon r'_o} \quad . \tag{30}$$

The quantities E_{ad} and E'_{ad} are the limiting activation energies for dissociation associated with the cases $x = 0$ and $y = 0$, respectively.

Using the expression $\sigma = n_{FT} e\mu$, the conductivity can be written as

$$\sigma = e\mu n_T^{1/2}[yn_\lambda e^{-2E_{ad}/k_B T} + xn'_\lambda e^{-2E'_{ad}/k_B T}]^{1/2} \tag{31}$$

Using the Einstein relation connecting the mobility μ and the diffusion coefficient D and recognizing that both quantities may have an activation energy E_{ah} associated with activated hopping, we can write

$$\mu = \frac{eD}{k_B T}$$

$$= \frac{eD_o}{k_B T} e^{-E_{ah}/k_B T} \qquad (32)$$

Substituting Eq. (32) into Eq. (31) and using definitions of n_λ and n'_λ, we see that a plot of $\ln(\sigma T^{3/2})$ versus $1/T$ for $x = 0$ or $y = 0$ should yield a straight line. Even when neither x nor y is zero, this plot should still be very close to a straight line. The slope of the line multiplied by $-k_B$ gives the effective activation energy for the conductivity, E_a.

The system that we are considering can be compared to that of an alkali halide such as NaCl doped with $CaCl_2$ or $CdCl_2$, which has been discussed previously.[12,13] The Ca^{++} or Cd^{++} ions substitute for Na^+ ions in the lattice, and to preserve electroneutrality positive ion vacancies must be introduced simultaneously with a concentration equal to that of Ca^{++} or Cd^{++}. Positive ion vacancies behave as negative charges which, when dissociated from the Ca^{++} or Cd^{++} ions, are mobile and can contribute to the electrical conductivity. The overall activation energy for the conductivity is the sum of a part connected with the dissociation of a positive ion vacancy from a divalent cation and a part connected with the diffusion of a positive ion vacancy under the influence of an applied electric field. In our system the mobile lithium ions are the analogues of the positive vacancies. In the standard treatment a positive ion vacancy is regarded as completely free unless it occupies one

of the twelve nearest-neighbor neighbor sites of a divalent cation. We make no such assumption in our treatment and take into account the Coulomb interaction at large distances of a Li^+ ion from a LiO^- or $LiSO_4^-$ ion.

1.2.3.3. Numerical Results and Comparison with Experiment

Numerical calculations of the conductivity as a function of temperature and composition were carried out in two ways: (i) the conductivity was calculated from the relation $\sigma = (n_F+n_F')e\mu$ using the exact expressions contained in Eqs. (7) and (8) and in Eqs. (16) and (17) to determine n_F and n_F', respectively; and (ii) the conductivity was calculated from Eq. (31) which is based on the approximations $\lambda \simeq r_i >> r_o, r_o'$. In both cases the parameter n_T was taken to be 1.0×10^{22} cm^{-3} and the parameters D_o, E_{ah}, and ε were varied to give the best least squares fit to the experimental data. The mobility activation energy E_{ah} was determined from the y=0 data (only Li_2O present) to be 0.38 eV and was kept at this same value for the y≠0 data (Li_2SO_4 present). The parameters D_o and ε were determined for each value of y.

The results are the following.

Case (i)

The quantity $\ln(\sigma T^{3/2})$ is plotted against the reciprocal of the absolute temperature in Figure 13 for each of the compositions y = 0.0, 0.05, 0.10, and 0.15. The theoretical curves are straight lines which fit the experimental data quite well except for some deviations at the two lowest temperatures. From the values of ε determined by the fits to the data, the values of the

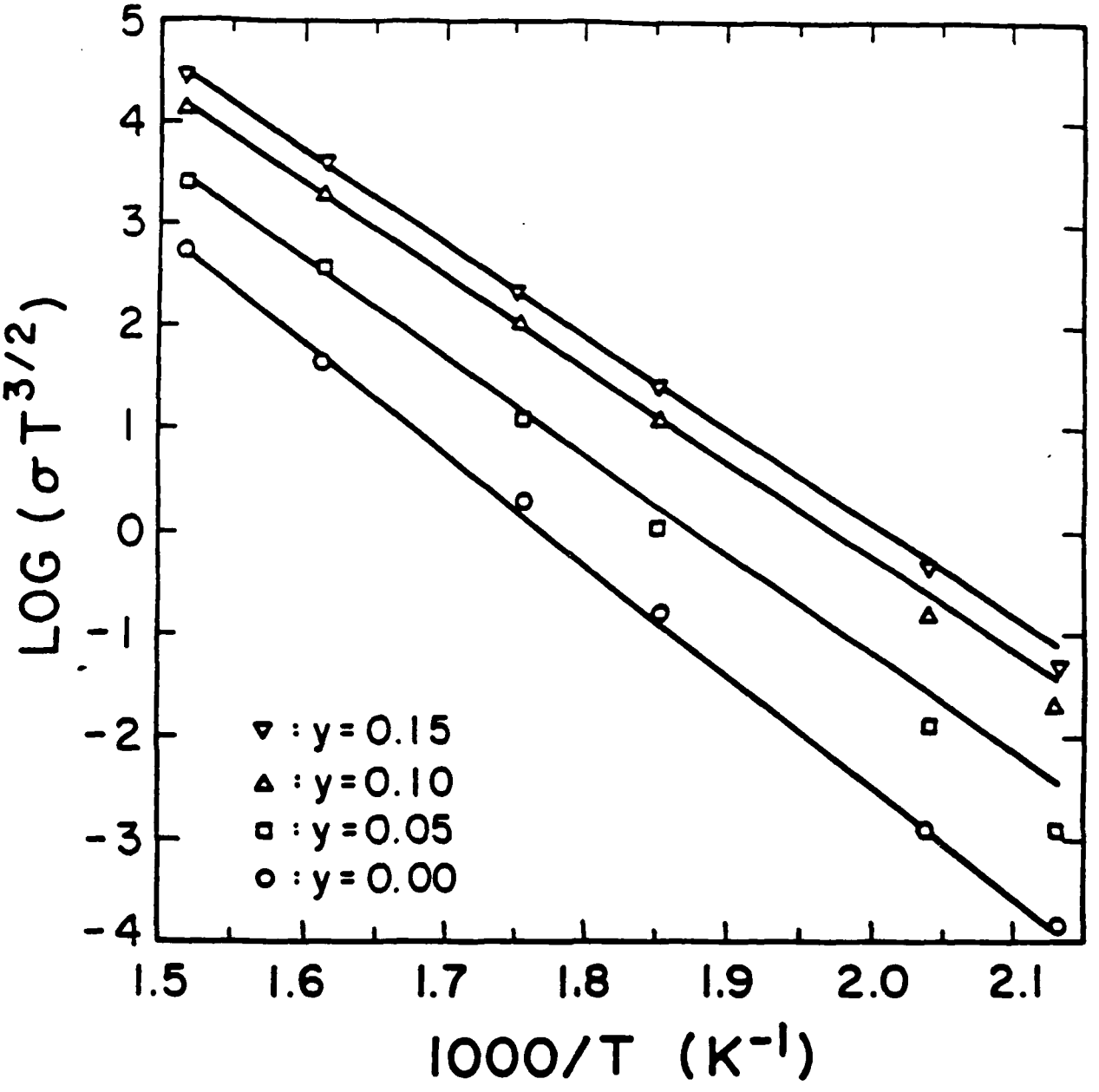

Figure 13. Variation of log ($\sigma T^{3/2}$) as a function of the reciprocal absolute temperature for different concentrations y of Li_2SO_4 in B_2O_3-0.5Li_2O-yLi_2SO_4. The theoretical results are represented by the solid curves.

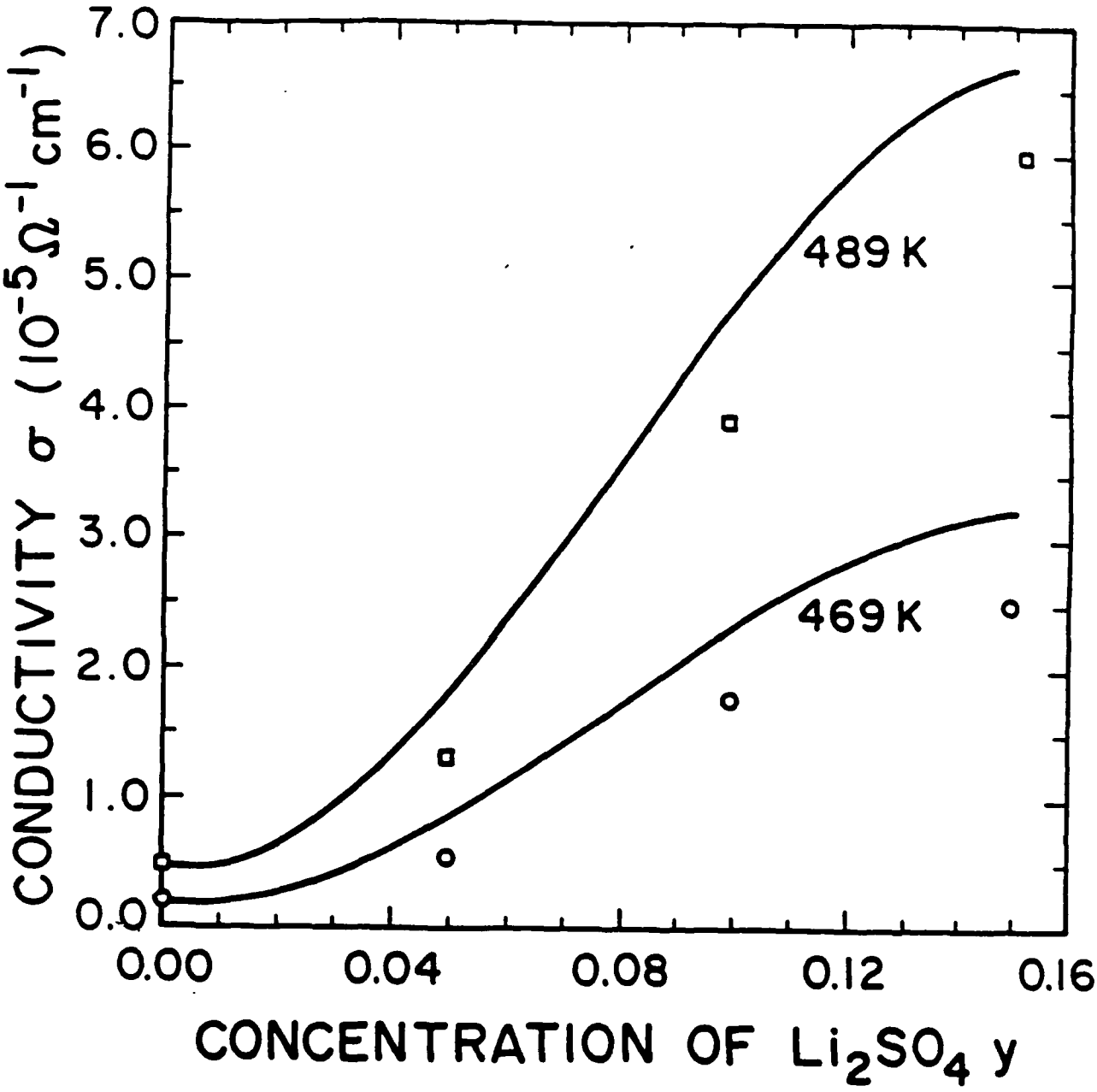

Figure 14a. Variation of the conductivity σ as a function of Li_2SO_4 concentration y for T = 469 K and 489 K.

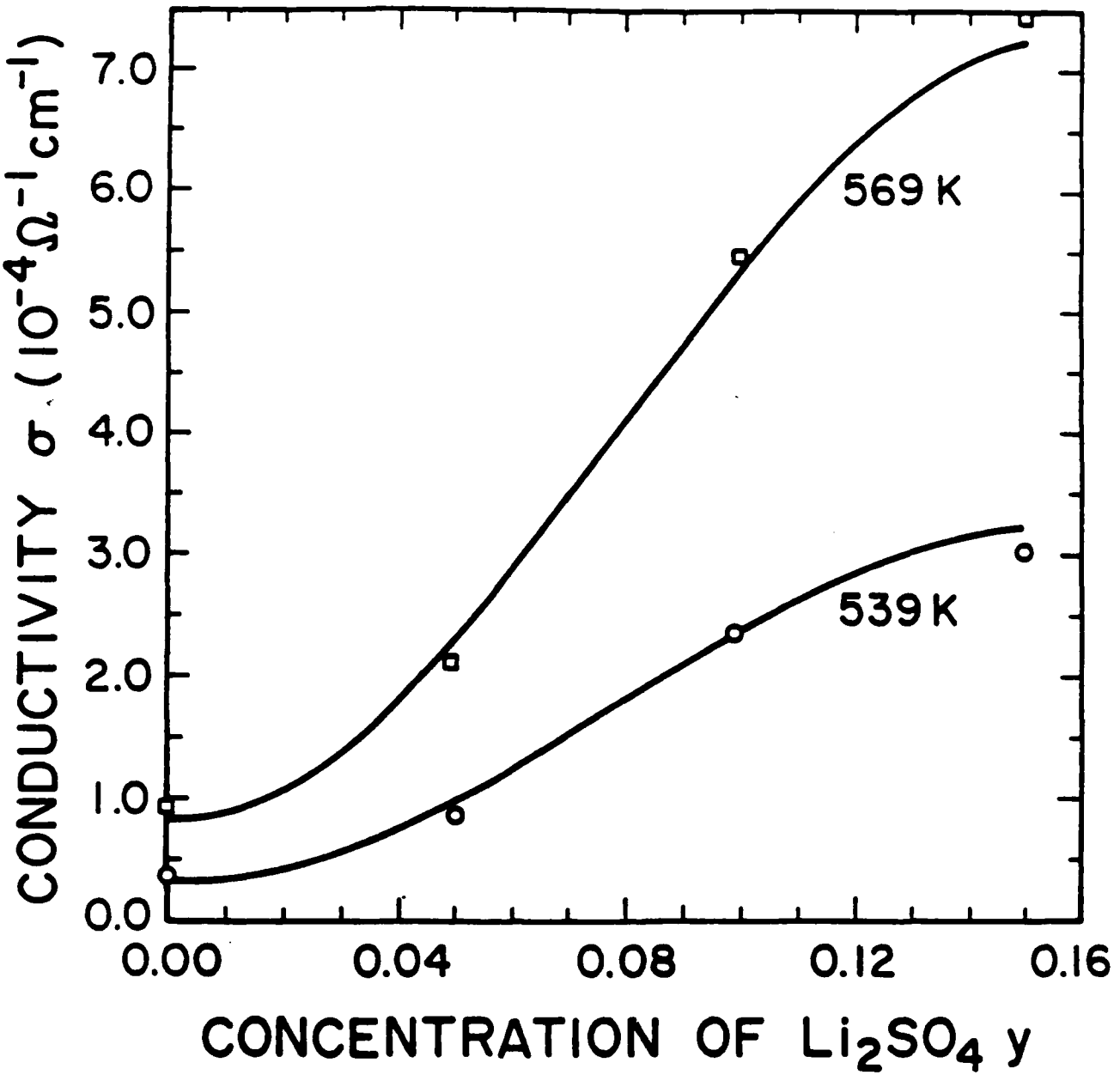

Figure 14b. Variation of the conductivity σ as a function of Li_2SO_4 concentration y for T = 539 K and 569 K.

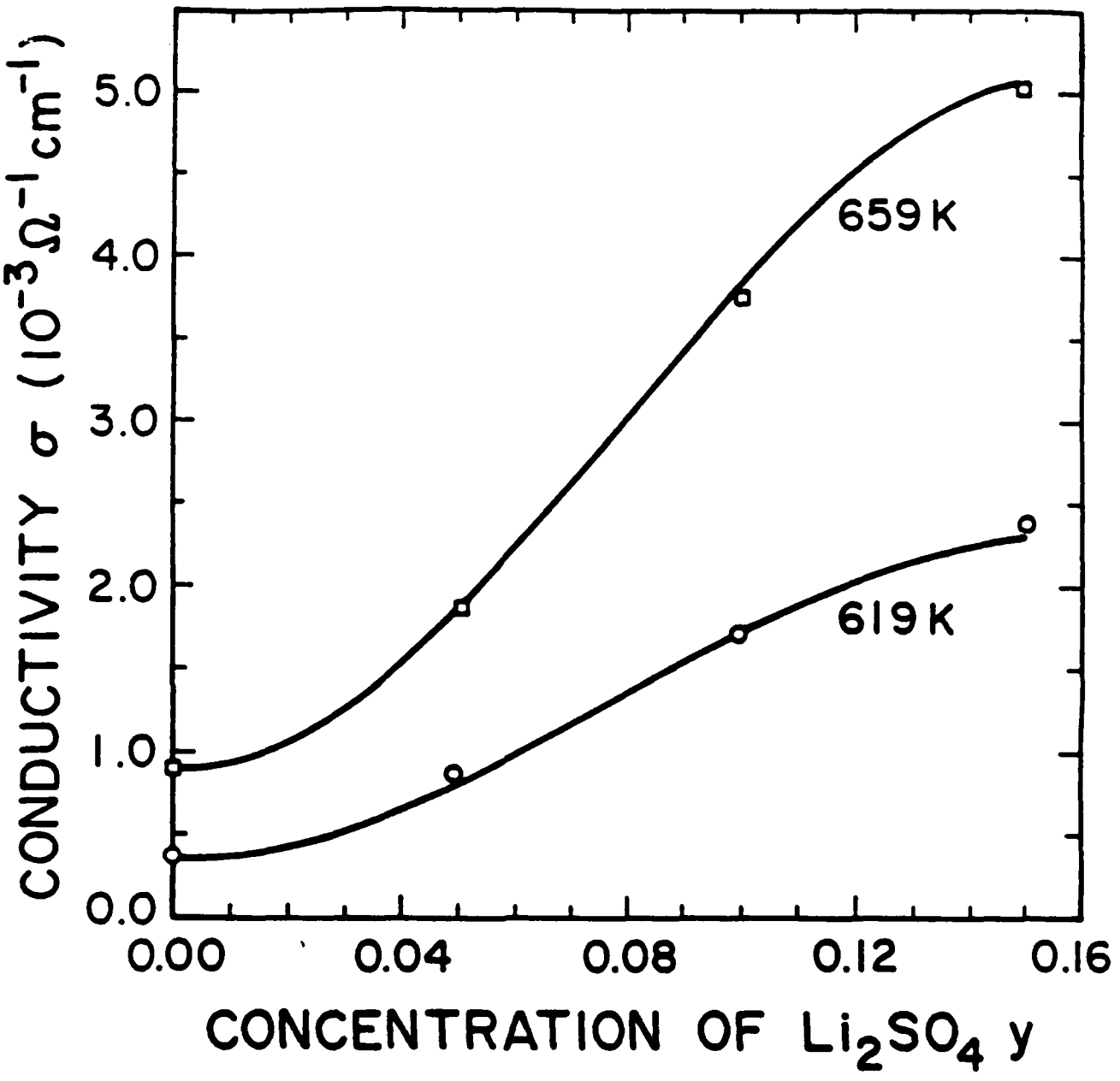

Figure 14c. Variation of the conductivity σ as a function of Li_2SO_4 concentration y for T = 619 K and 659 K.

dissociation activation energies E_{ad} and E'_{ad} were calculated using Eqs. (29) and (30). The overall activation energy E_a was determined from the slopes of the theoretical curves in Figure 13. The results for D_o, ε, E_{ad}, E'_{ad}, and the theoretical and experimental values of E_{aA} are presented in Table 2. We see that the four quantities D_o, ε, and E_{ad}, and E'_{ad} show only a weak dependence on the composition variable y, and their magnitudes are physically reasonable. That of D_o conforms roughly to the relation[12] $D_o = \nu_+ r_h^2/6$ where ν_+ and r_h are the hopping frequency and hopping distance, respectively. Taking 0.2 cm^2 sec^{-1} as a representative value of D_o from Table 2 and taking[12] $\nu_+ = 10^{14}$ sec^{-1}, we find that $r_h \approx 11$ A, a not unreasonable value.

The conductivity σ is plotted against y in Figure 14 for the temperatures 469K, 489K, 539K, 569K, 619K, and 659K. As in Figure 13 there are appreciable deviations between theory and experiment for the two lowest temperatures, but for the four highest temperatures the agreement is good. One can, of course, improve the agreement for the two lowest temperatures by making ε temperature dependent.

Case (ii)

When the conductivity σ is calculated using Eq. (31), the plots of $\ln(\sigma T^{3/2})$ versus 1/T fall within one percent of those given in Figure 13 for case (i) for each value of y. Plots of σ versus y also fall within one percent of those given in Figure 14 for case (i). These results indicate that the approximations underlying Eq. (31) are well satisfied.

TABLE 2

CONDUCTIVITY PARAMETERS FOR B_2O_3-xLi_2O-yLi_2SO_4

y	D_0	ε	E_{ad}	E_{ad}'	E_a (theor.)	E_a (exp.)
0.00	0.15	6.6		0.55	0.93	0.93
0.05	0.26	6.0	0.44	0.60	0.83	0.90
0.10	0.21	6.5	0.41	0.55	0.79	0.83
0.15	0.21	6.6	0.40	0.55	0.78	0.83

The theory[14] which we have developed for the dissociation of Li_2SO_4 in lithium borate glasses B_2O_3-Li_2O gives a good representation of the dependence of the conductivity on the Li_2SO_4 content and on the temperature. By comparing the experimentally determined conductivity with the theoretical results one obtains information concerning the activation energy associated with the mobility, the diffusion constant and the dielectric constant.

1.2.3.4. Coulomb Interaction between Free Li^+ Ions

The effect of the Coulomb interaction between free Li^+ ions can be taken into account by using the Debye-Hückel theory in a form applied by Lidiard[13] to a similar problem. What has to be done is to replace the dissociation constants K(T) and K'(T) by $K_{DH}(T)$ and $K'_{DH}(T)$ given by

$$K_{DH}(T) = \frac{1}{n_\lambda} \exp\{\frac{\lambda}{r_o} - \frac{1}{2}[(2\lambda)^{3/2}(4\pi n_{FT})^{1/2} \frac{1}{1+\kappa r_o}]\} \qquad (33)$$

$$K'_{DH}(T) = \frac{1}{n'_\lambda} \exp\{\frac{\lambda}{r'_o} - \frac{1}{2}[(2\lambda)^{3/2}(4\pi n_{FT})^{1/2} \frac{1}{1+\kappa r'_o}]\} \qquad (34)$$

where $\kappa^2 = 8\pi n_{FT}\lambda$. Since the new equilibrium constants involve n_{FT}, the mass action law equations are now transcendental equations for the determination of n_{FT} and must be solved self-consistently.

If we introduce the quantities $n = n_o + n_B$ and $n' = n'_o + n'_B$ which are, respectively, the total concentrations of Li_2SO_4 and Li_2O, we can rewrite Eqs. (23) and (24) in the form

$$n_o = \frac{n}{1+n_{FT}K_{DH}(T)} \tag{35}$$

$$n_o' = \frac{n'}{1+n_{FT}K_{DH}'(T)} \quad . \tag{36}$$

Using conservation of lithium ions, we have

$$n_{FT} = n_o + n_o'$$

$$= \frac{n}{1+n_{FT}K_{DH}(T)} + \frac{n'}{1+n_{FT}K_{DH}'(T)} \quad . \tag{37}$$

Equation (37) is the equation that must be solved self consistently to give the total free Li^+ ion concentration n_{FT}.

Once n_{FT} is found, we can determine the conductivity σ using the relation

$$\sigma = e\mu n_{FT} \tag{38}$$

where μ is the mobility. In the presence of the Coulomb interaction between the free Li^+ ions, the mobility μ_n for the noninteracting case must be multiplied by a factor ζ given by

$$\zeta = \frac{nf}{n+n'} + \frac{n'f'}{n+n'} \tag{39}$$

where

$$f = 1 - \frac{\lambda\kappa}{3(\sqrt{2}+1)(1+\kappa r_o)(\sqrt{2}+\kappa r_o)} \tag{40a}$$

$$f' = 1 - \frac{\lambda\kappa}{3(\sqrt{2}+1)(1+\kappa r_o')(\sqrt{2}+\kappa r_o')} \quad . \tag{40b}$$

The expression for the conductivity then takes the form

$$\sigma = e\mu_n \zeta n_{FT} \quad . \tag{41}$$

We have used Eqs. (37) and (41) to calculate the conductivity for the system B_2O_3-0.5Li_2O-yLi_2SO_4 as a function of y and the temperature T. The values of the parameters ε, r_o, and r_o' used here are: $\varepsilon = 6.5$, $r_o = 2.70$Å, $r_o' = 2.0$Å. The results are presented in Figures 15, 16, and 17 for the various compositions and temperatures considered. At the two lowest temperatures, there is a small, but distinct lowering of the conductivity that arises from the Coulomb interaction between the free Li^+ ions. A given ion is slowed up by its interaction with its ion atmosphere. As the temperature increases, the lowering of the conductivity diminishes and is hardly evident at the two highest temperatures. This behavior can be understood on the basis that an increase in temperature increases the random thermal motion of the free Li^+ ions and reduces the correlations that arise from the Coulomb interaction between them. These results are consistent with the picture that the lithium borate glasses behave as weak electrolytes with only a small fraction of the Li_2O and Li_2SO_4 molecules ionized at the temperatures employed in the experiments.

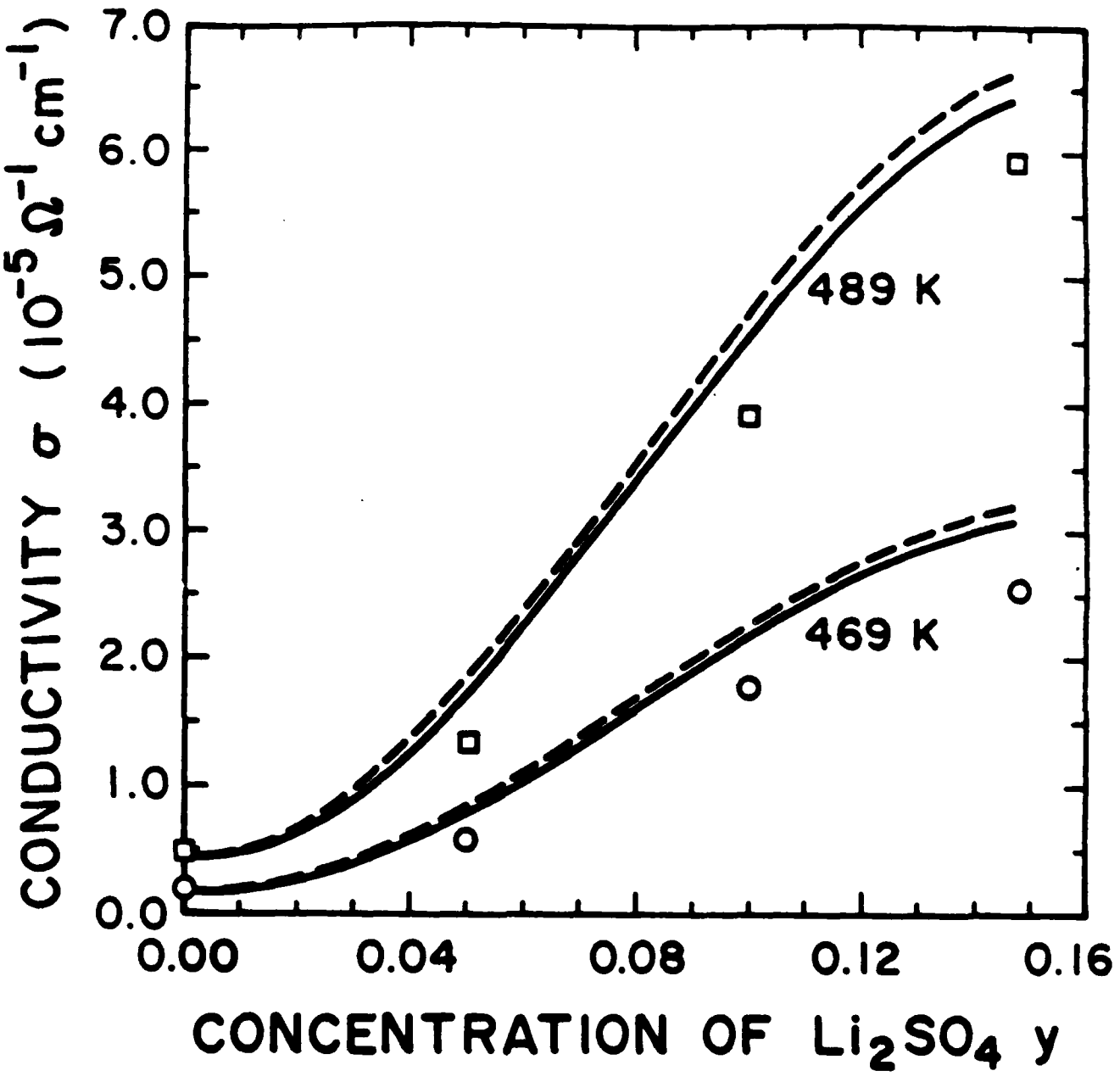

Figure 15. Variation of the conductivity σ as a function of Li_2SO_4 concentration y for T = 469 K and 489 K. The solid and dashed lines are the cases with and without inclusion of the interaction between free Li^+ ions, respectively.

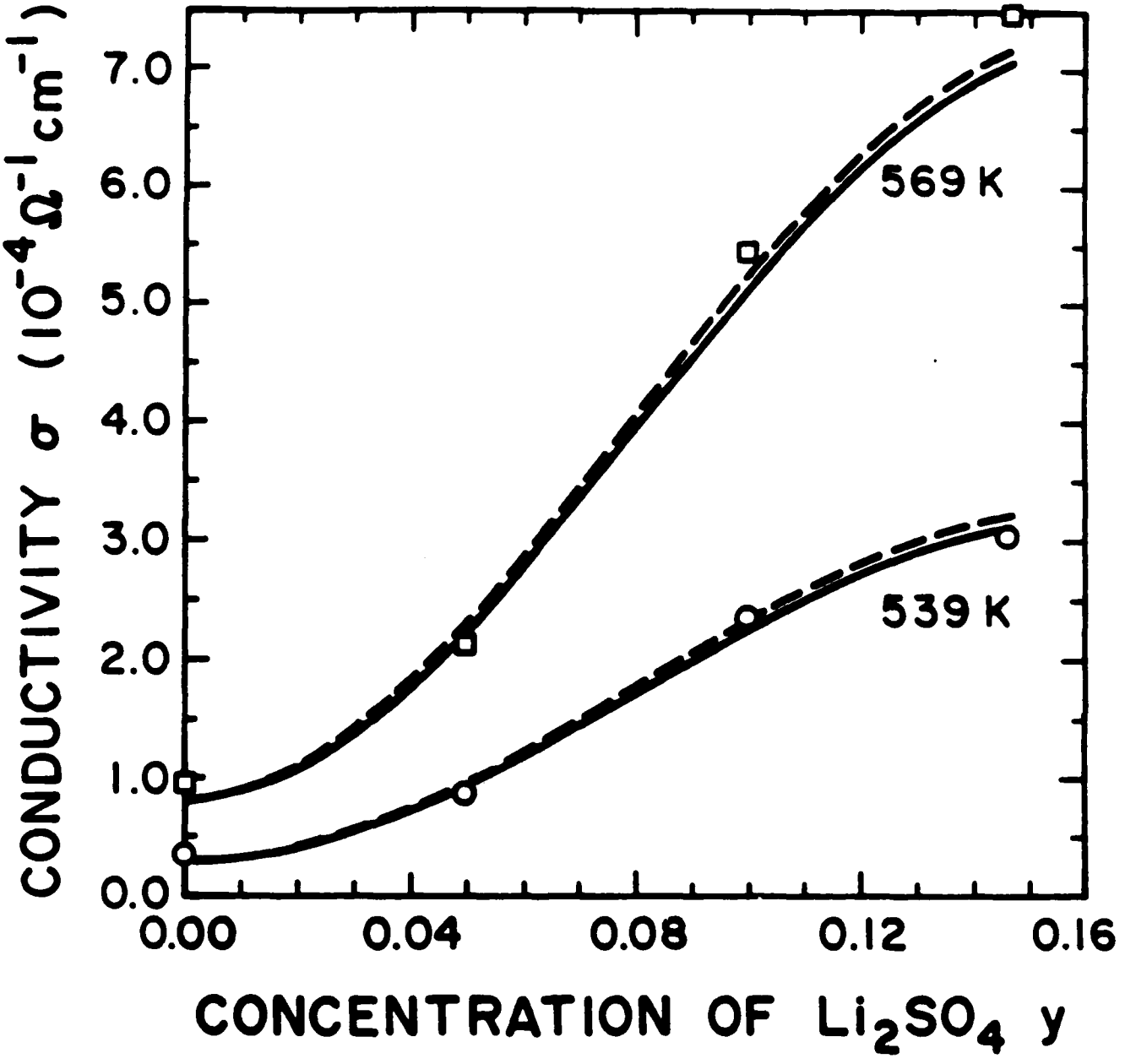

Figure 16. Variation of the conductivity σ as a function of Li_2SO_4 concentration y for T = 539 K and 569 K. The solid and dashed lines are the cases with and without inclusion of the interaction between free Li^+ ions, respectively.

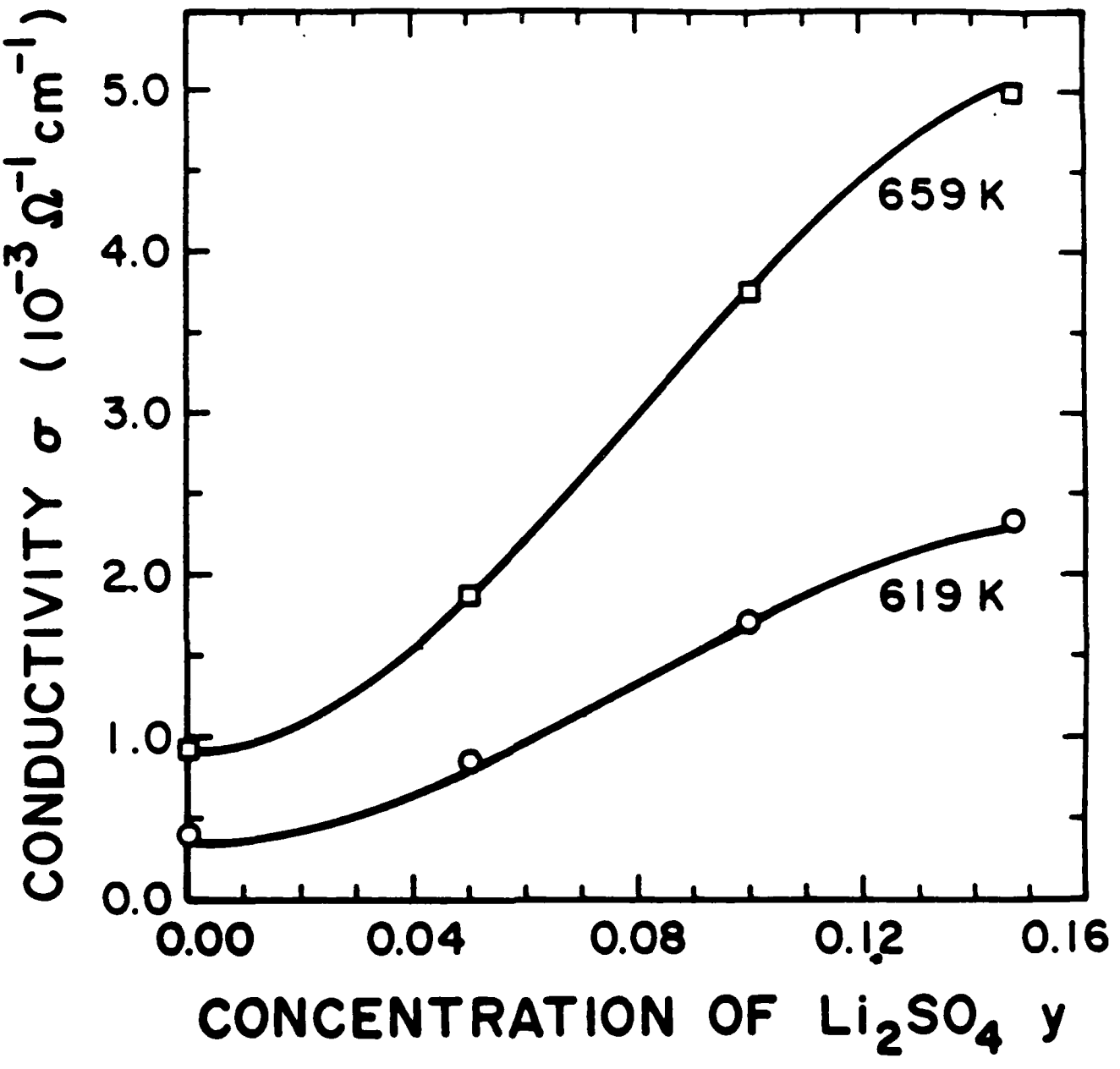

Figure 17. Variation of the conductivity σ as a function of Li_2SO_4 concentration y for T = 619 K and 659 K. The cases with and without inclusion of the interaction between free Li^+ ions are indistinguishable.

1.3. Lithium Ion Vibration in Borate Glasses

In the discussion of the dynamics of the Li^+ ions we shall refer to the borate glass structure shown in Figure 1.

Reflectivity measurements were performed with a Bruker Infrared Fourier Transform Spectrometer (IFS) at room temperature. The spectral range analyzed is 50 to 2000 cm^{-1}, the sample used on parallelepipeds of dimensions 8x8x4 mm.

Infrared reflectivity spectra for B_2O_3-0.7Li_2O-yLi_2SO_4 at T=300K are shown in Figure 18. In the spectrum corresponding to the composition x=0.7, y=0 three main features are identified at 1400 cm^{-1}, 1000 cm^{-1}, and 700 cm^{-1} associated with the infrared active vibrational modes of BO_3, BO_4 and B-O-B, respectively. Addition of the dopant Li_2SO_4 introduces two new bands at 600 cm^{-1} and 1100 cm^{-1} associated with the ν_4 and ν_3 modes of the sulfate ion SO_4^{--}:

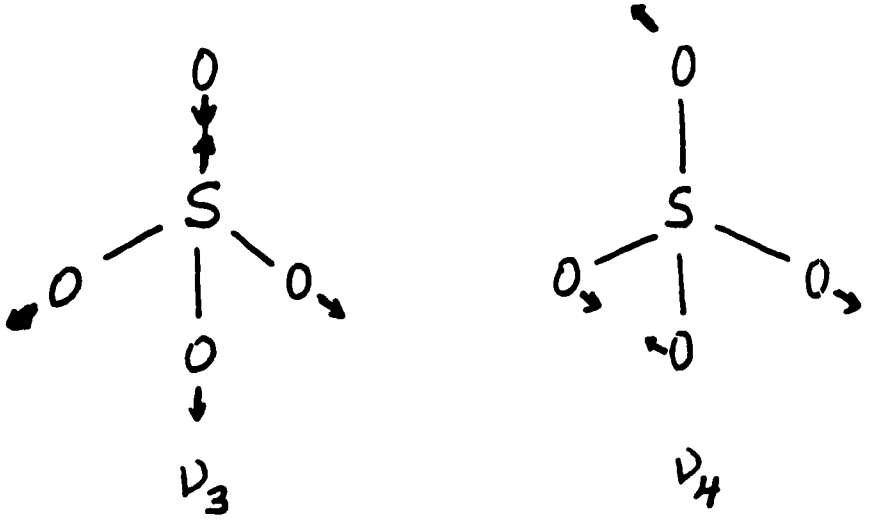

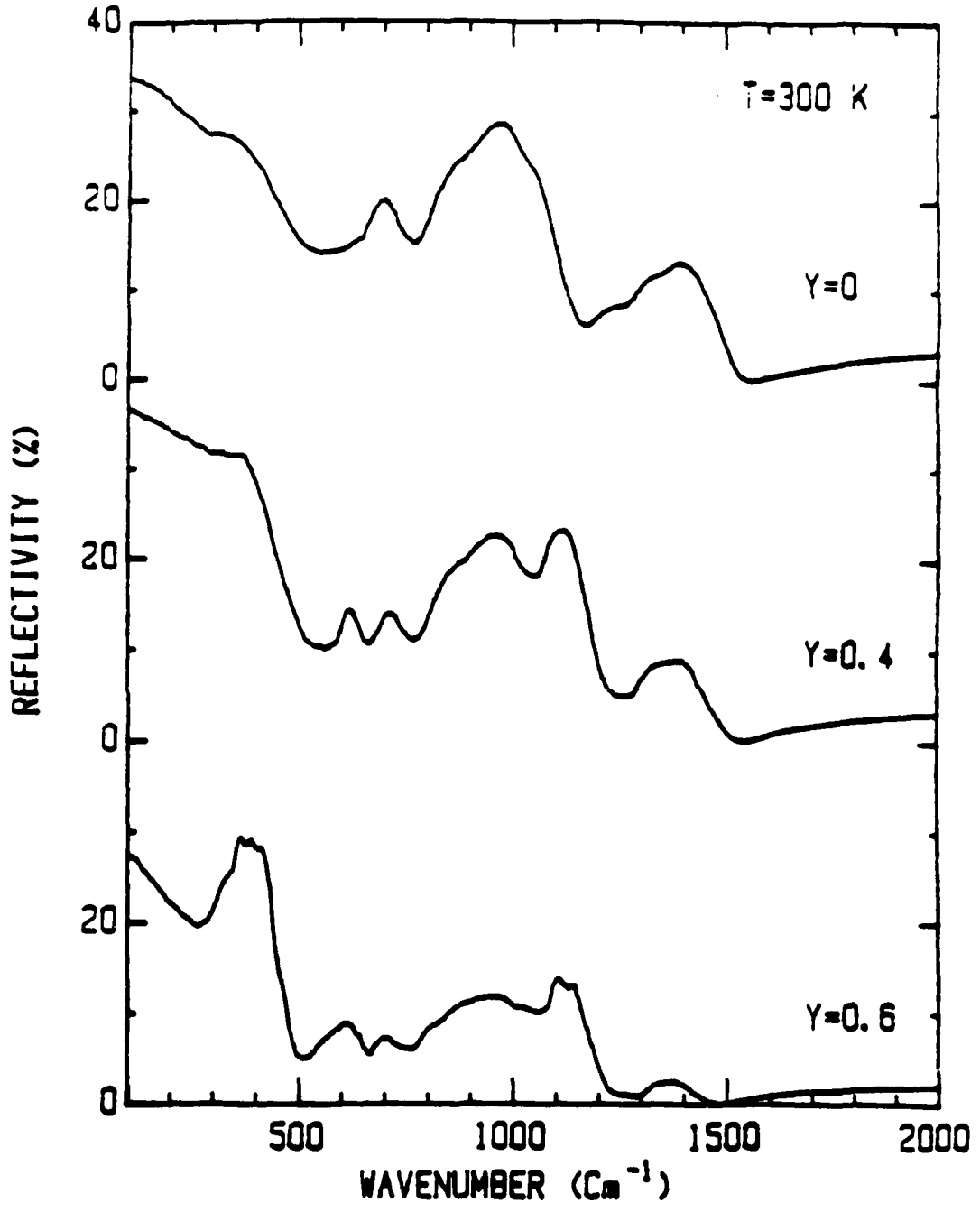

Figure 18. Infrared reflectivity spectra for B_2O_3-0.7Li_2O-yLi_2SO_4 at T = 300K.

The band which corresponds to the Li vibration at 400 cm^{-1} is covered by a broad band probably due to the molecular reorientation in the system (Debye relaxation).

In order to analyze the reflectivity spectra it is necessary to perform a Kramers-Kronig transformation to get the optical constants associated with each of the vibrational modes. In Figure 19 is shown the imaginary part of the dielectric constant associated with the transverse optical phonon (TO) mode. The vibrational frequency of a Li^+ ion is situated at 380 cm^{-1}. This vibration concerns essentially the Li^+ -O bonds of the vitreous matrix.

In Figure 20 is presented the frequency dependent conductivity which shows a resonance at a frequency close to 380 cm^{-1}. The shapes of the spectra for doped and undoped samples are similar which is consistent with the fact that B_2O_3-Li_2O is also a Li^+ conductor. This result also shows that there is practically no difference in the structure of B_2O_3-0.7Li_2O and B_2O_3-0.7Li_2O-0.4Li_2SO_4 which indicates that for concentrations $y<0.4$ the dominant Li sites are the same.

2. LITHIUM INTERCALATION IN InSe

2.1. Characteristics of the Intercalation Process

2.2.1. Introduction

Lithium intercalation in InSe single crystals has been performed[15] for the first time in the Laboratoire de Physique des Solides of the Université Pierre et Marie Curie, Paris. Chemical insertion of Li in InSe is obtained by insertion of a single crystal of InSe in a 1.6 M solution of n-butyllithium in

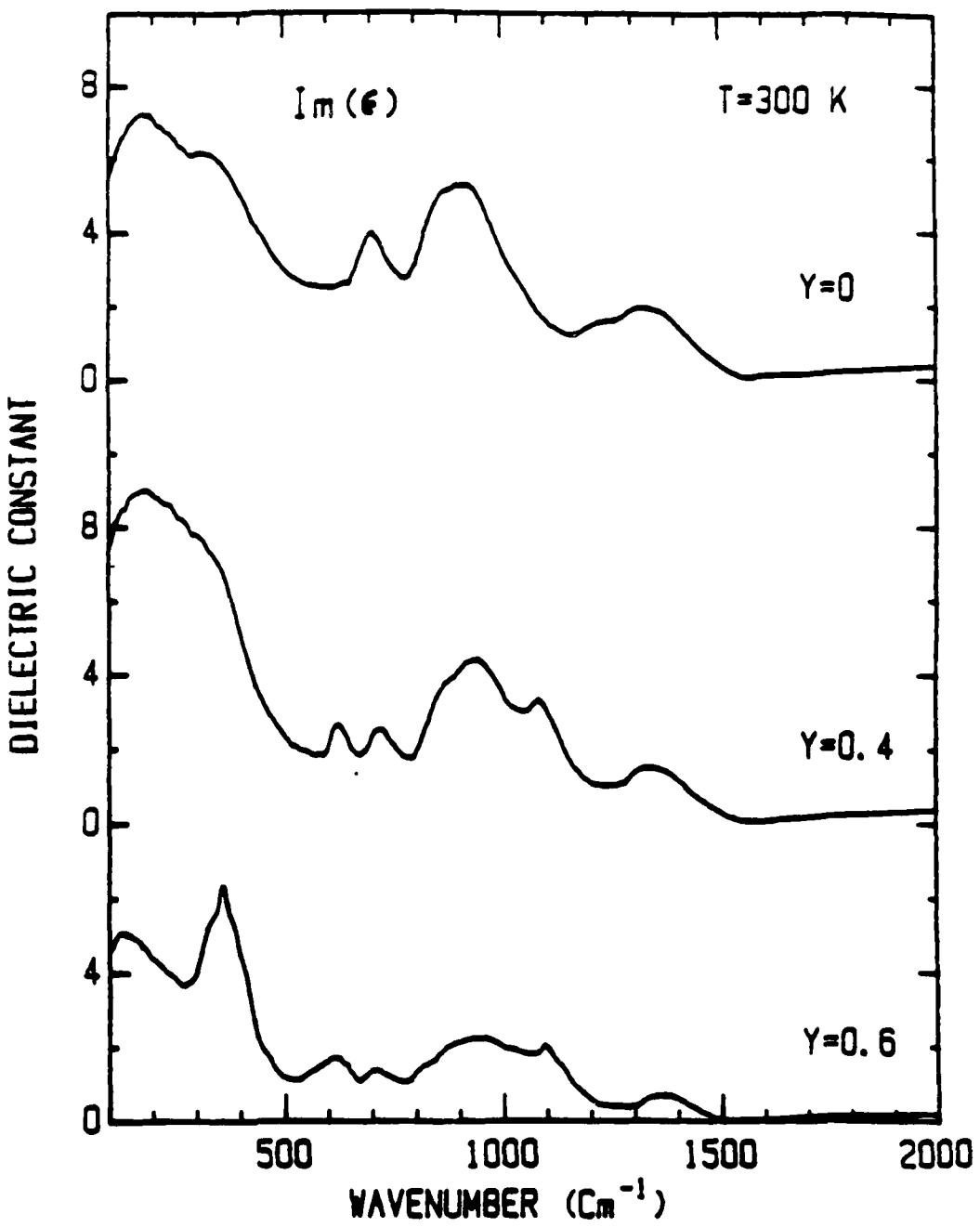

Figure 19. Imaginary part of the dielectric constant for B_2O_3-0.7Li_2O-yLi_2SO_4 at T = 300 K.

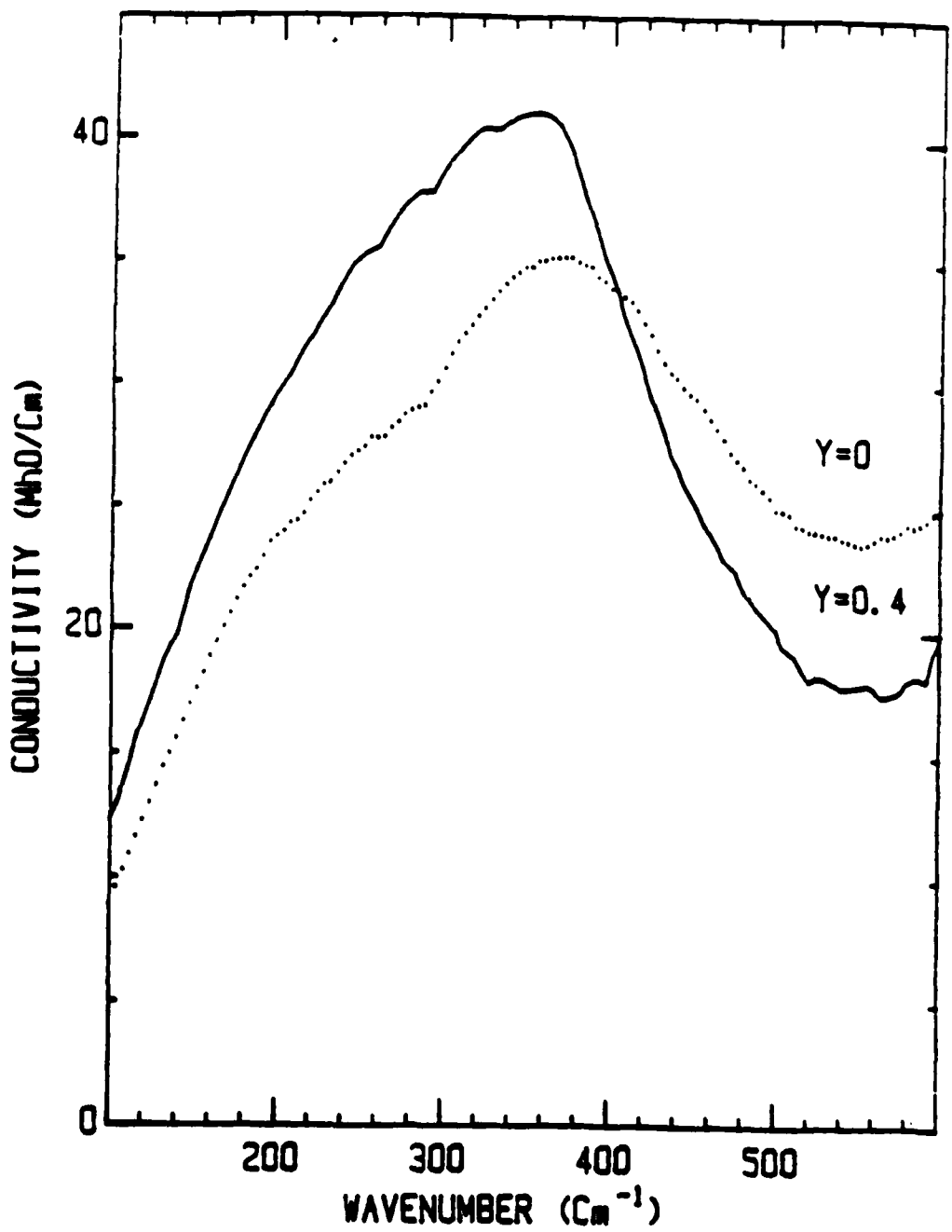

Figure 20. Frequency dependent conductivity for B_2O_3-0.7Li_2O-yLi_2SO_4.

hexane. Spontaneous intercalation is produced under these conditions according to the reaction.

$$n - C_4H_9Li + InSe \rightarrow Li_xInSe + \frac{1}{2}\ n\text{-}C_8H_{18}.$$

The reaction lasts for a long time under an inert atmosphere.

The following steps should be distinguished in this reaction.

l) pre-equilibrium in the solution generating the active species: monomer, dimer and trimer of $n\text{-}C_4H_9Li$

ii) surface adsorption and activation of the adsorbant ($n\text{-}C_4H_9Li$)

iii) electron transfer $e \rightarrow Li$ bound to the solid

iv) diffusion of Li into the lattice

v) ionization of Li

vi) dimerisation, diffusion of the alkane in the solution and production of octane.

The positions of the Li ions in the Van der Waals gaps of InSe are shown in Figure 21:

No indication of staging has been observed in this process of intercalation, but a saturation as a function of time has been observed. When lithium is intercalated into the layer compound InSe, electrical conductivity measurements indicate that the rate of intercalation is large at first, then decreases, and finally approaches zero. This behavior indicates that there is a maximum or saturation value of the lithium concentration that can be achieved. A physical picture of this saturation behavior is as follows. The lithium atoms enter the Van der Waals gap between adjacent InSe layers. The 2S electrons of the lithium atoms

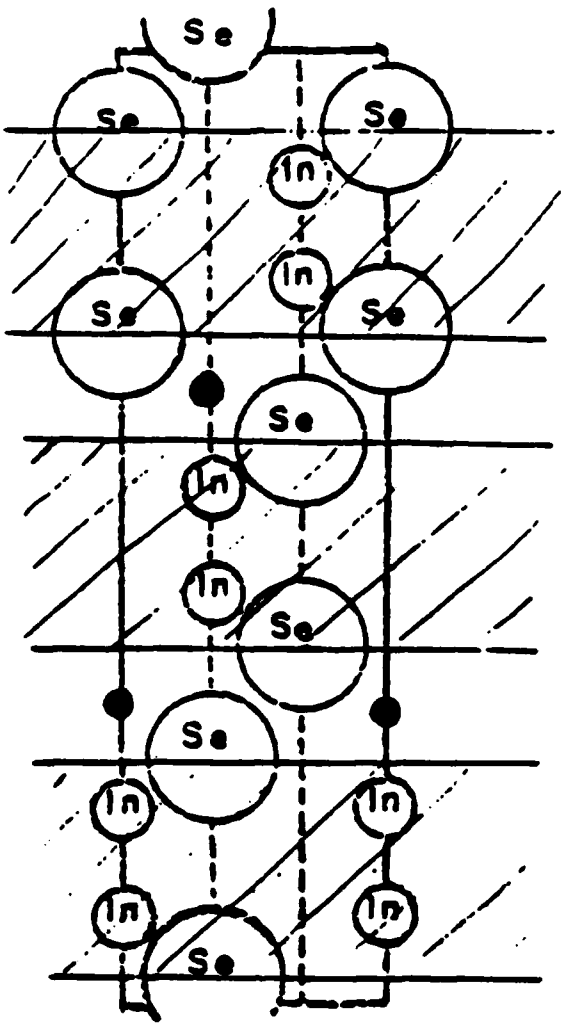

Figure 21. Positions of Li^+ ions (solid circles) in the Van der Waals gap.

ionize and transfer to a two-dimensional potential well in one of the adjacent InSe layers. As more lithium atoms are intercalated, the Fermi energy E_F of the electrons in the potential well rises as a consequence of the Fermi-Dirac statistics obeyed by the electrons. When the Fermi energy becomes equal to the energy of a 2S electron in a lithium atom, the transfer of electrons from the atoms to the potential well will cease and the electrical conductivity due to the electrons in the potential well will saturate.

2.1.2. Time Evolution of Intercalation

The intercalation of Li into InSe is achieved by immersing a single crystal of InSe into a 1.6 M solution off n-butyllithium in hexane. Experimental measurements of the resistivity of the InSe during intercalation have been made by C. Julien and coworkers in the laboratory of Professor M. Balkanski in Paris. The results for the resistivity as a function of time of intercalation are shown in Figure 22. It can be seen that the resistivity initially drops quite rapidly and then levels off. One might surmise that saturation is being approached at the largest times. However, this does not seem to be the case. One must beware of the logarithmic scale used on the vertical axis in Figure 22. If one plots the reciprocal of the resistivity, or conductivity, versus time of intercalation, one obtains the plot shown in Figure 23. We see that the conductivity is very nearly a linear function of time over the interval considered and that no evidence of saturation is shown. Viewed in this light, the experimental data are consistent with the picture that the

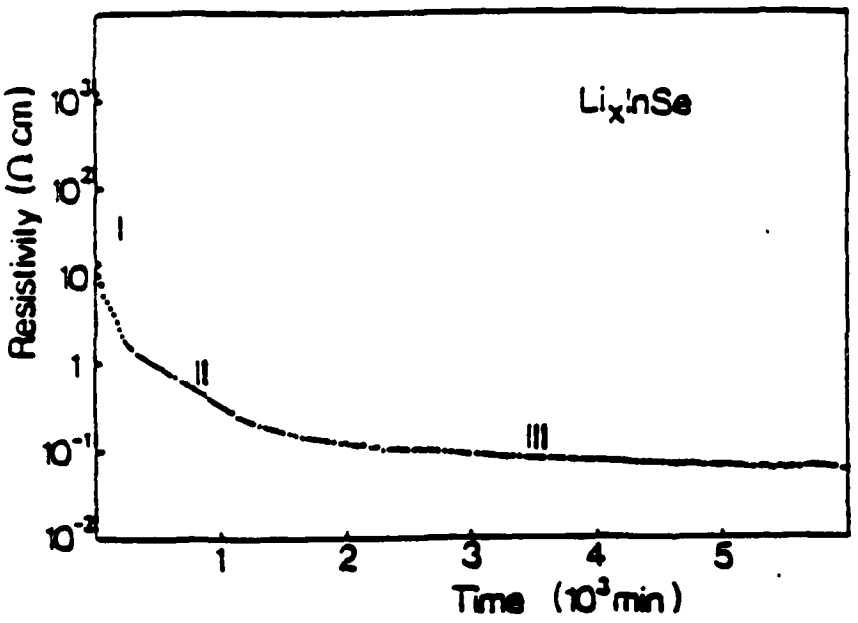

Figure 22. Resistivity versus time curve during Li-InSe intercalation at room temperature.

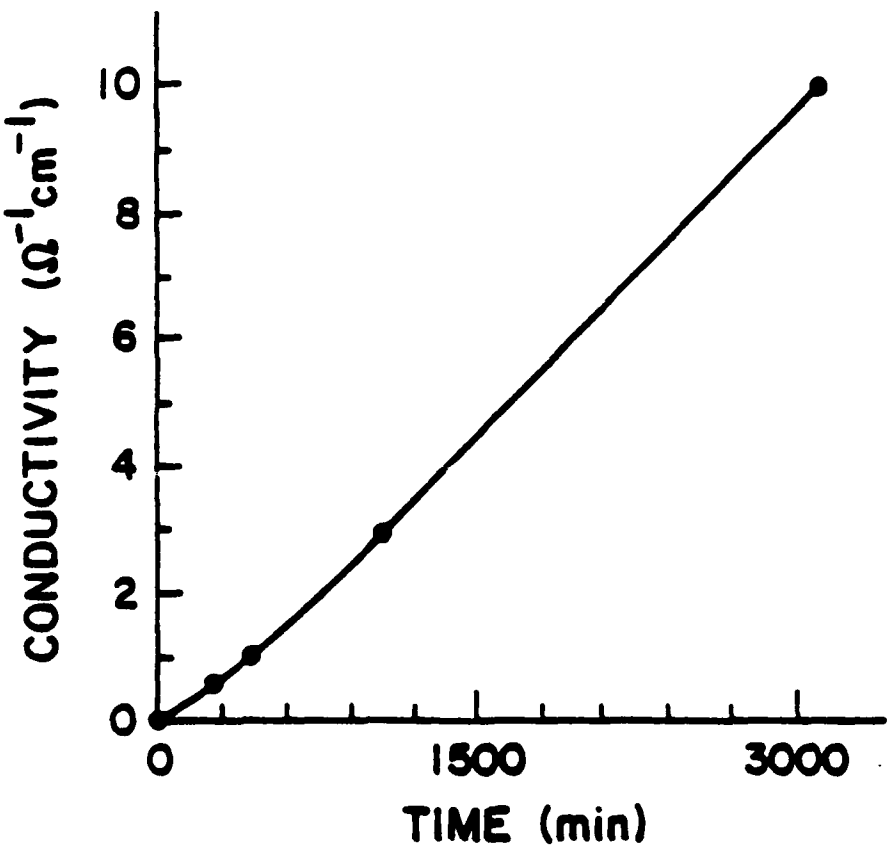

Figure 23. Conductivity versus time curve during Li-InSe intercalation at room temperature.

conduction electron concentration in the InSe is increasing linearly with time as a consequence of a corresponding linear increase in Li concentration with time.

2.1.3. Analysis of Saturation of Electrical Conductivity During Intercalation

Although saturation of the conductivity has not yet been achieved experimentally, it should be attainable after sufficiently long periods of intercalation. In our physical picture, the intercalated Li atoms enter the Van der Waals gap between adjacent InSe layers and lose their 2S electrons to one or the other of the two-dimensional potential wells in the adjacent InSe layers. As more Li atoms are intercalated, the Fermi energy E_F of the electrons in the potential well rises as a consequence of the Fermi-Dirac statistics obeyed by the electrons. When the Fermi energy becomes equal to the energy of a 2S electron in a lithium atom, the transfer of electrons from the atoms to the potential well will cease and the electrical conductivity due to the electrons in the potential well will saturate.

We have carried out a Thomas-Fermi analysis of the fraction of electrons transferred as a function of the well depth. Let the width of the Van der Waals gap be a_o and the periodicity length perpendicular to the planes of the InSe be c_o. The quantity c_o-a_o is therefore the width of the potential well. Within the well, the potential has the constant value V_o. The Li^+ ions are assumed to be uniformly distributed over two planes symmetrically disposed about the middle of the Van der Waals gap

and a distance C_+ apart.

The Thomas-Fermi procedure utilizes an energy functional of the electron number density which consists of the kinetic energy and electrostatic potential energy. By minimizing the energy function with respect to variations in number density, one obtains a relation between the latter and the electric potential. Combining this relation with Poisson's equation and applying the appropriate boundary conditions leads to an expression for the number density as a function of position in the system. The fraction of the electrons located within the InSe potential well can then be readily calculated, and the result is (details of the calculation can be found in R&D status report No. 3 for contract No. F33615-85-K-2501).

$$f = \frac{Q_2}{Q_1 + Q_2}$$

$$= \left(\cosh \frac{\alpha_o}{2} \bar{\tau} + \frac{V_o}{p_o} \sinh \frac{\alpha_o}{2} \bar{\tau}\right) \frac{\sinh \frac{c-\alpha_o}{2} \bar{\tau}}{\sinh \frac{c}{2} \bar{\tau}} \qquad (42)$$

where Q_1 is the electron charge in the Van der Waals gap, Q_2 is that in the InSe layer, $\alpha_o = \frac{a_o}{a_B}$, $a_B \equiv \frac{\hbar^2}{me^2}$ is the Bohr radius, $\bar{\varepsilon}$ is the mean dielectric constant and $\bar{\tau}^2 = \frac{2\mu}{c\bar{\varepsilon}}$ with $\mu = \frac{m^*}{m}$ the reduced electron mass and $c = \frac{c_o}{a_B}$.

The fraction f increases with increasing potential well depth V_o until a critical value of V_o is reached for which f = 1 and all of the electrons have been transferred from the lithium atoms to the InSe layer. In Figure 24 is given a plot of f versus

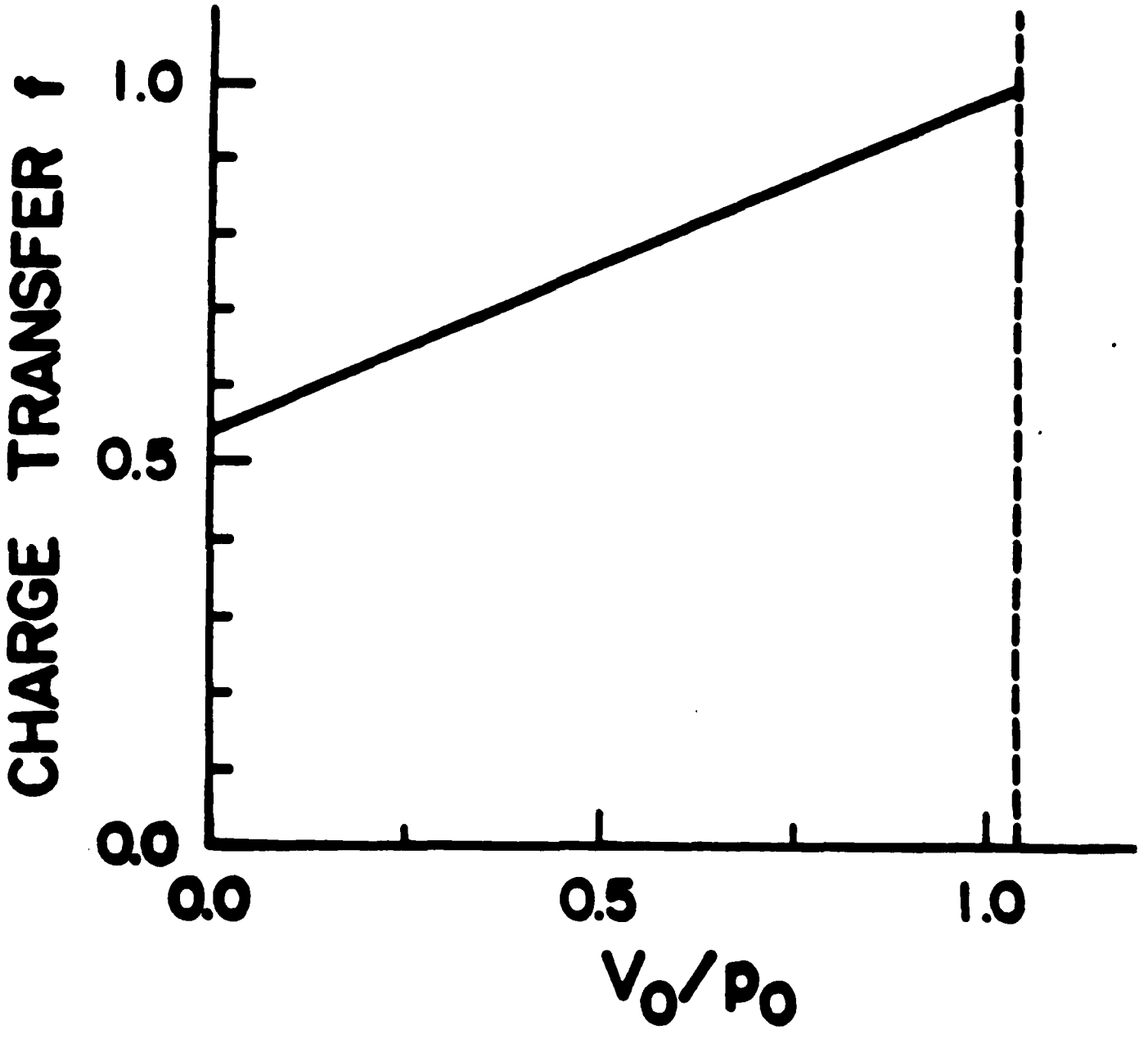

Figure 24. Charge transfer at saturation versus potential well depth for Li-InSe intercalation.

V_o/p_o. We see that f increases linearly with V_o. The critical value of V_o is found to be $V_{crit} = 1.043\ p_o$. The minimum value of f is not zero because the Li^+ ions are assumed to be at the interface between Van der Waals gap and the InSe layer. A more realistic calculation is currently underway in which the Li^+ ions are moved into the Van der Waals gap away from the interface.

2.2. Tight Binding Calculation of the Energy Bands in InSe

The first step in calculating the potential energy surface is to obtain the electronic wave functions and energy eigenvalues of InSe. To this end, we have set up a tight binding calculation of the energy bands in InSe. The tight binding parameters were taken to be those of Doni et al., Il Nuovo Cimento 51B, 154 (1979). The results for the energy bands are in agreement with those of Doni et al., so the computer code is believed to be correct.

2.2.1. Tight Binding Calculation of the Potential Energy Surface for Lithium Ions in InSe

The activation energy is the energy difference between a local potential energy minimum of a lithium ion and the saddle point between that minimum and the next one. It is therefore necessary to calculate the potential energy surface for the motion of a lithium ion in InSe in order to obtain the activation energy. We have carried out such a calculation using the Thomas-Fermi approximation in which the potential $\Phi(\vec{r})$ at a given point in the crystal is related to the electron density at that point by the relation

$$\Phi(\vec{r}) = -\frac{\hbar^2}{2me}\left[3\pi^2\rho(\vec{r})\right]^{2/3} \tag{43}$$

where $\rho(\vec{r})$ is the electron density at the point $\vec{r}$. The density can be expressed in terms of the Bloch functions $\psi_{\vec{k},t}(\vec{r})$ as

$$\rho(\vec{r}) = \sum_{\vec{k},t} \phi^*_{\vec{k},t}(\vec{r})\,\psi_{\vec{k},t}(\vec{r}) \tag{44}$$

where $\vec{k}$ is the wave vector and t denotes the atomic orbital associated with the Bloch state. The Bloch functions are obtained using the tight binding method and are given in terms of the atomic orbitals $\psi_t(\vec{r}-\vec{R}_j)$ by

$$\psi_{\vec{k},t}(\vec{r}) = C \sum_j \psi_t(\vec{r}-\vec{R}_j)e^{i\vec{k}\cdot\vec{R}_j} \tag{45}$$

where $\vec{R}_j$ is the position vector of the j-th atomic site and C is the normalization constant. The atomic orbitals were taken to be those tabulated by Herman and Skillman[16], and the tight binding parameters were taken to be those of Doni et al.(17).

Using the Bloch functions for $\vec{k} = 0$, the electron density $\rho(\vec{r})$ was calculated using Eq. (44). The potential $\Phi(\vec{r})$ was then calculated using Eq. (43). The potential energy $V(\vec{r})$ is given by $V(\vec{r}) = e\Phi(\vec{r})$. A contour plot of the potential energy as a function of position in the unit cell is given in Figure 25 for the plane lying in the center of the Van der Waals gap between successive InSe layers. The positions of minimum potential energy are indicated by squares, and the saddle point corresponding to the minimum activation energy for ion motion is

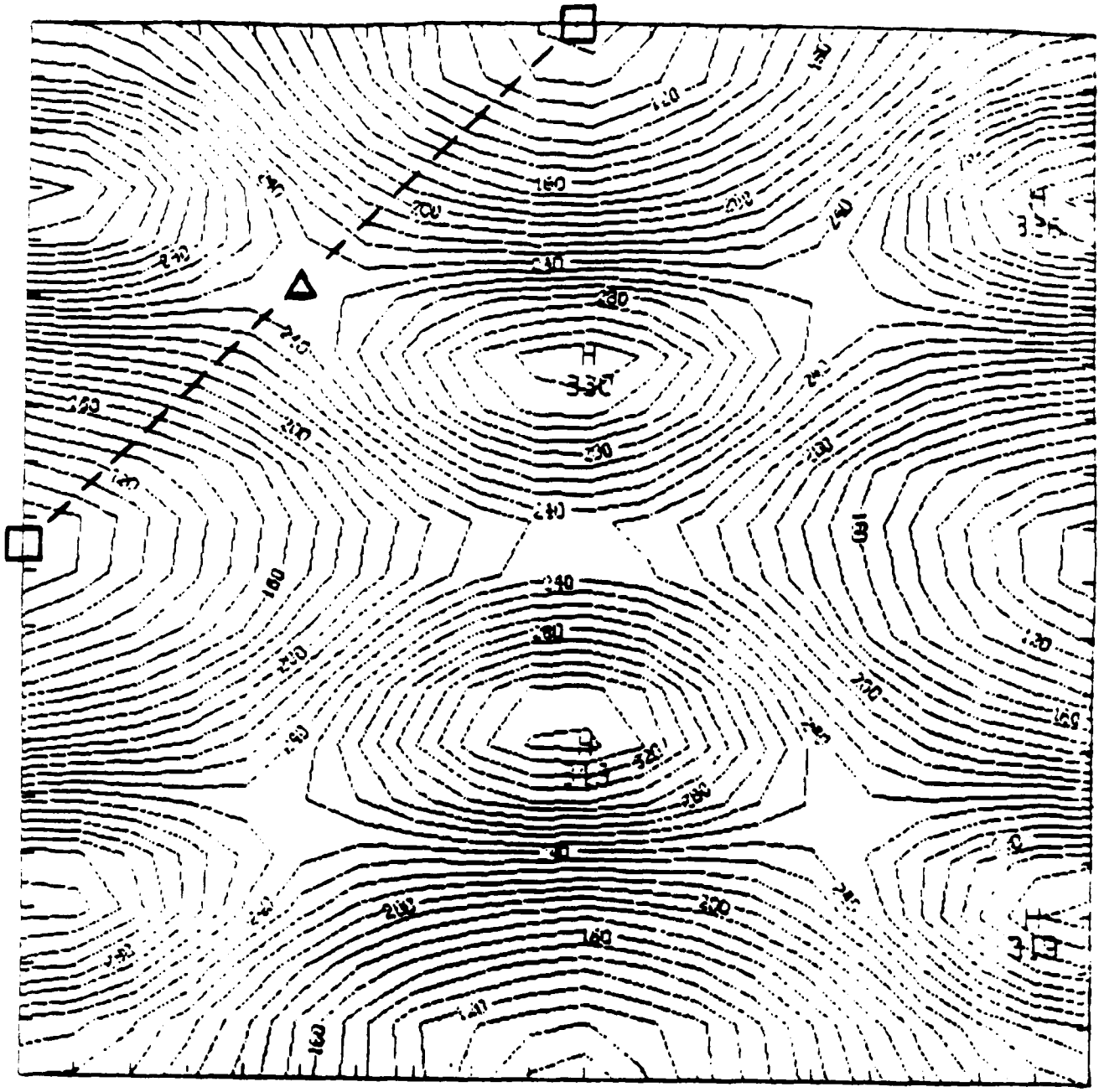

Figure 25. Potential energy contours for a lithium ion moving in the plane of the Van der Waals gap of InSe. The regions of high potential energy are selenium atoms. □ :potential minimum; Δ: saddle point.

indicated by the triangle. The contours are labeled by the energies in Rydbergs. The activation energy is the difference in energy of the sites labeled by squares and triangles and is found to be 2.2 eV.

We feel that the activation energy just quoted is rather large in view of the apparent ease with which intercalated lithium atoms move through the InSe lattice. This calculation was repeated by taking into account all values of the wave vector $\vec{k}$ in the first Brillouin zone. A new contour plot is obtained as shown in Figure 26. The potential energy along the path from one minimum to the next through the saddle point is shown in Figure 27. From this plot the activation energy can be seen to be 1.6 eV, which is significantly smaller than the value of 2.2 eV obtained using only the $\vec{k} = 0$ Bloch functions.

The 1.6 eV value is still rather large in view of the apparent ease with which intercalated lithium atoms move through the InSe lattice. Since we have up to now neglected the 2s electron of the lithium atom, it seems appropriate that we include it in our calculations.

3. FAST ION TRANSFER BETWEEN LITHIUM BORATE GLASS AND InSe LAYER COMPOUND

3.1.' Introduction

In the solid state battery concept based on a doped lithium borate glass as the electrolyte and indium selenide intercalated with lithium as the cathode, the borate glass is a three-dimensional fast ion conductor whereas the indium selenide is a two-dimensional fast ion conductor with the lithium ions moving

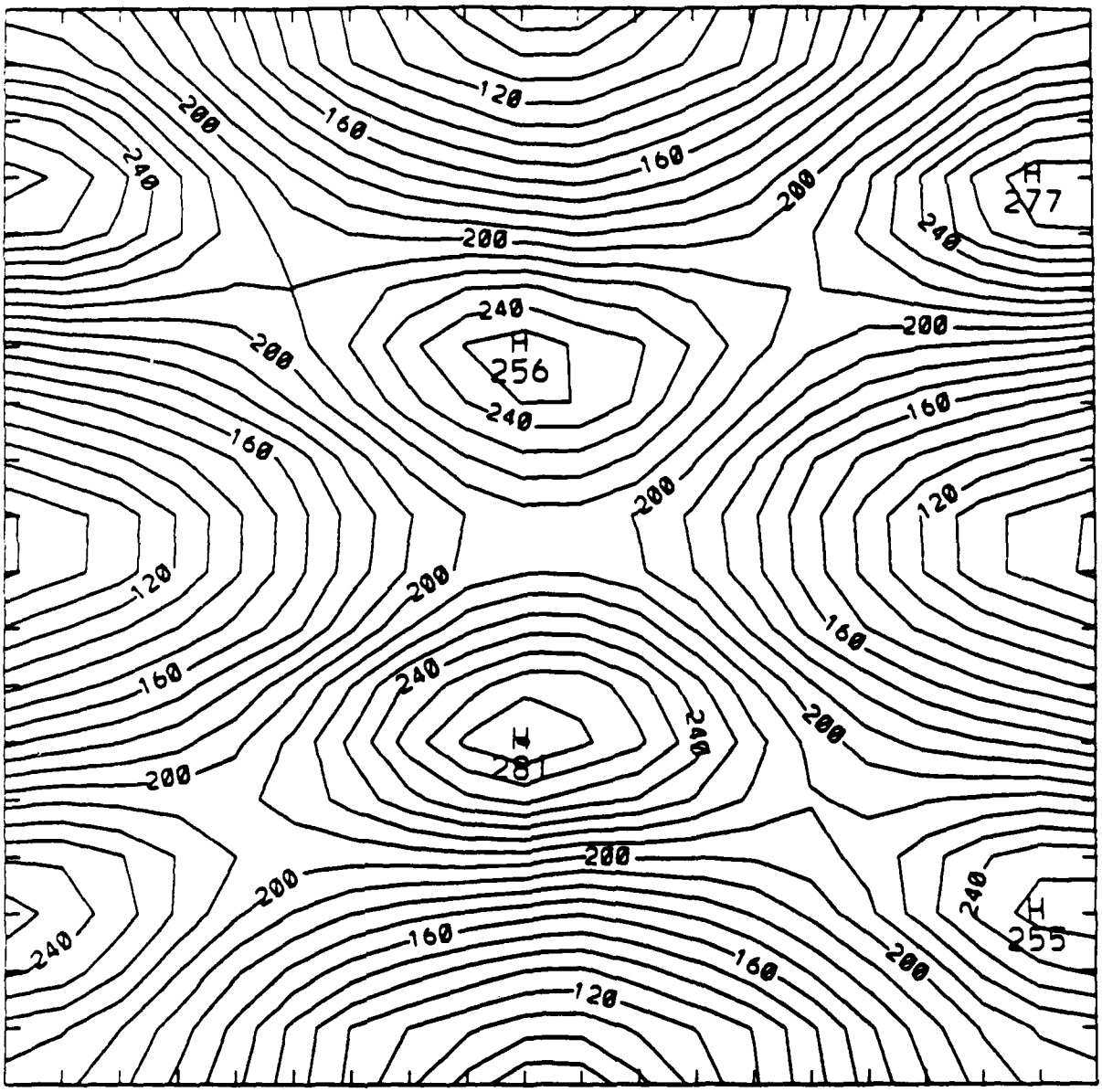

Figure 26. The new potential energy contours for a lithium ion moving in the plane of the Van der Waals gap of InSe when all values of the wave vector $\vec{k}$ in the first Brillouin zone are taken into account. The regions of high potential energy are selenium atoms.

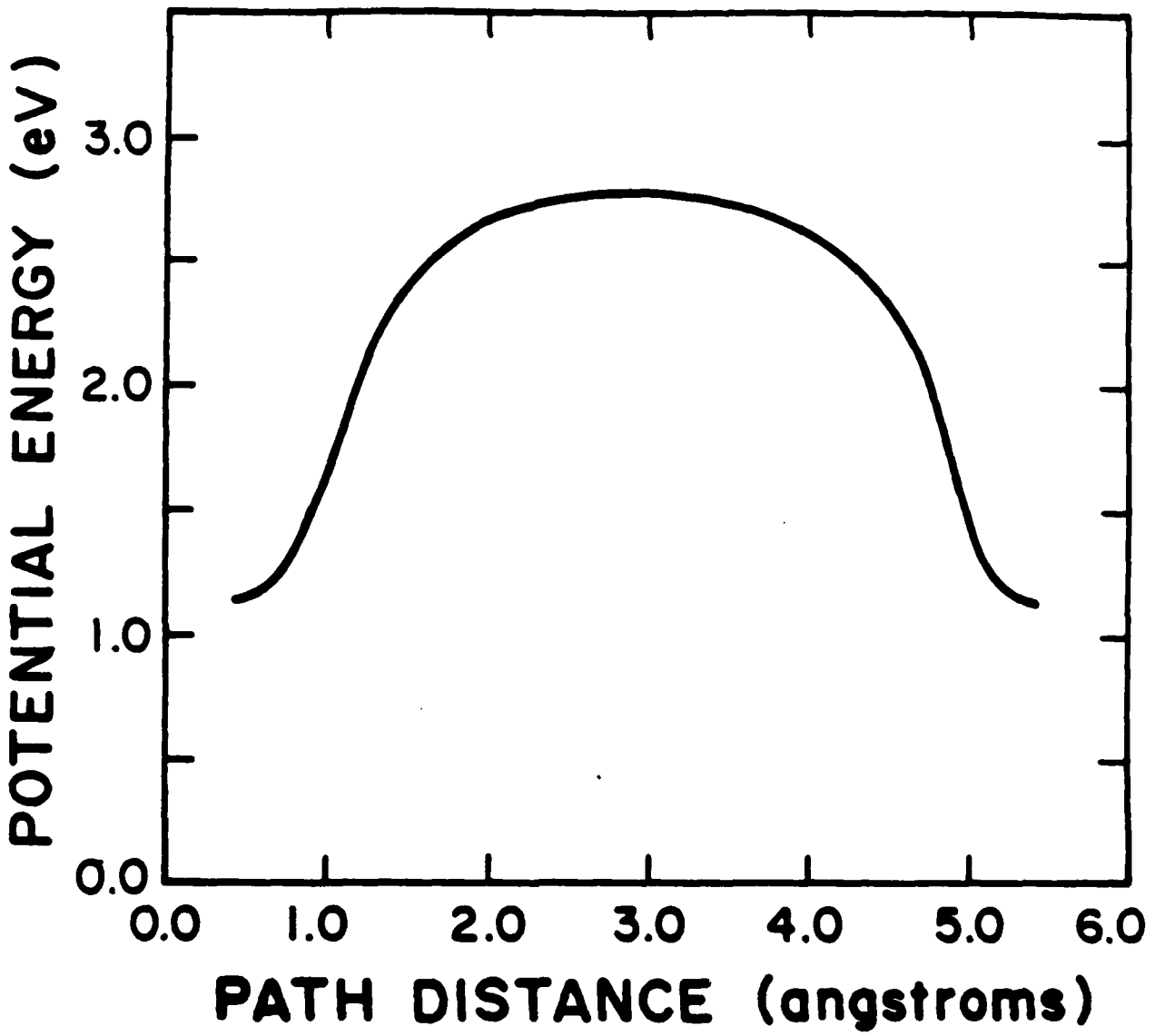

Figure 27. The potential energy along the path from one minimum to the next through the saddle point.

in the Van der Waals gaps between the InSe layers. The ion current must therefore make a transition from three-dimensional to two-dimensional behavior as the Li^+ ions pass from the glass into the InSe.

In Section 1.2, we presented a theory of the electrical conductivity of a lithium borate glass doped with Li_2SO_4. The conductivity as a function of temperature and composition was calculated and found to be in good agreement with experimental data. In this chapter, we give the results of a theoretical investigation of the constant current contours and constant potential contours for the flow of positive ions from the glass into the InSe under the influence of an applied voltage. The effective resistance of the glass as a function of the geometrical parameters is also calculated.

3.2. Theoretical Development

The geometry of our system is shown in Figure 28. The Van der Waals gaps in the InSe have width 2c and the distance between successive Van der Waals gaps is 2w. A slab of borate glass of width 2w and length L can be viewed as centered against each Van der Waals gap. A potential difference $\Delta\phi$ is imposed across the borate glass as shown. We require that the Li^+ ions enter the InSe only through the Van der Waals gaps. The borate glass is assumed to have a conductivity σ.

The problem we address is to calculate the current density J in the borate glass as a function of c, w, L and $\Delta\phi$. We proceed by solving Laplace's equation

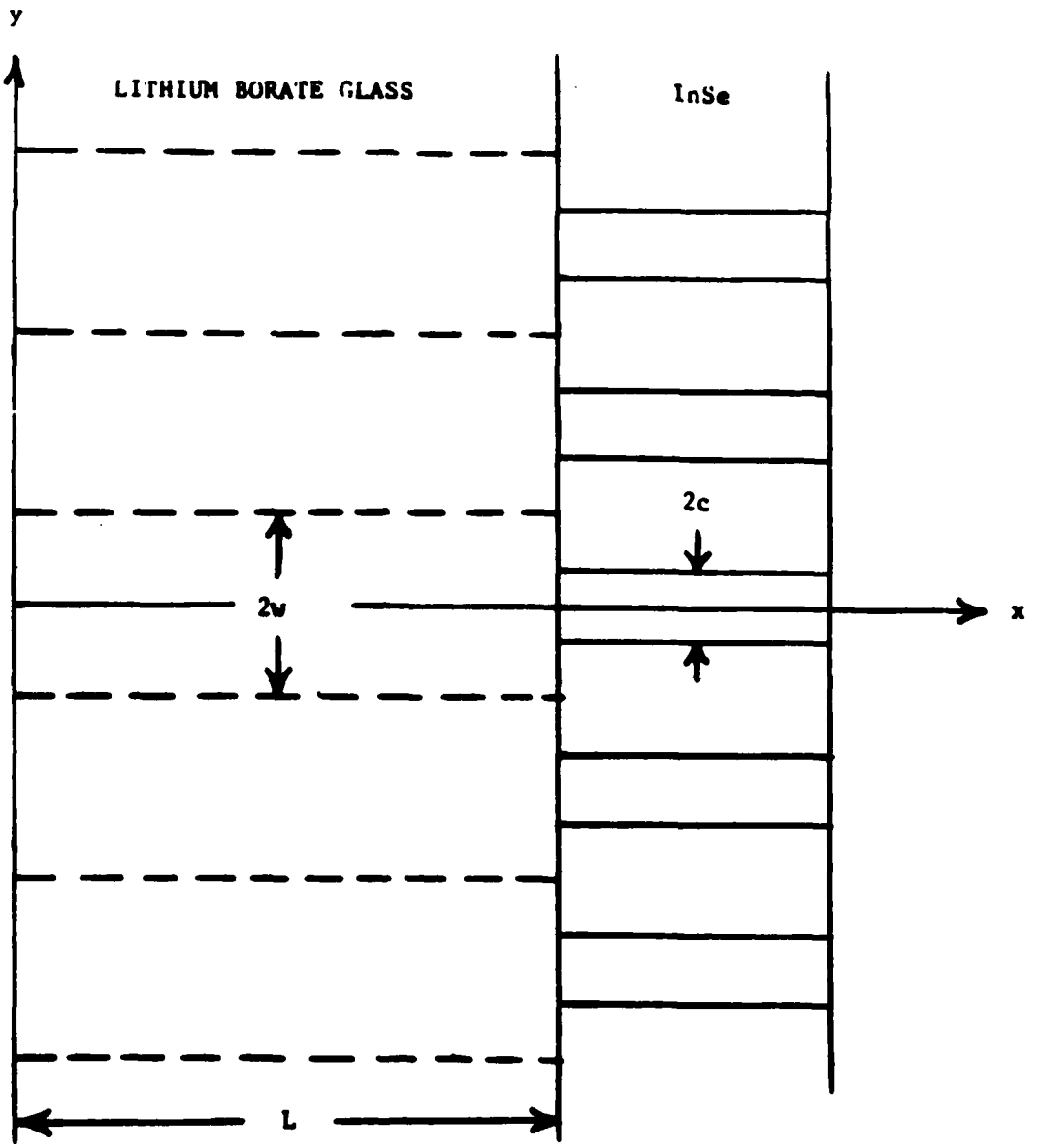

Figure 28. Diagram of the lithium borate glass - InSe system.

$$\Delta^2\phi = 0 \tag{46}$$

subject to appropriate boundary conditions. If we assume that the system extends to $\pm \infty$ in the y-direction, we can exploit the periodicity of the system by utilizing Fourier series.

The boundary conditions which the potential $\phi(x,y)$ satisfies are the following:

$$\phi(0,y) = \phi_a \tag{47a}$$

$$\phi(L,y) = \phi_b \tag{47b}$$

$$\left.\frac{\partial\phi(x,y)}{\partial x}\right|_{x=L} = \begin{cases} -J_o/\sigma & \text{for } |y| < c \\ 0 & \text{for } c < |y| < w \end{cases} \tag{47c}$$

$$\left.\frac{\partial\phi(x,y)}{\partial y}\right|_{y=\pm w} = 0 \text{ for } 0 < x < L \tag{47d}$$

where J_o is the current density across a Van der Waals gap of InSe at the interface with the lithium borate glass. The solution of Eq. (46) which satisfies Eqs. (47) can be expressed in the form

$$\phi(x,y) = \phi_a - (J_o/\sigma)\left[\frac{c}{w}x + \frac{2w}{\pi^2}\sum_{n=1}^{\infty}\frac{1}{n^2}\cdot\frac{\sinh\frac{n\pi x}{w}\cos\frac{n\pi y}{w}\sin\frac{n\pi c}{w}}{\cosh\frac{n\pi L}{w}}\right] . \tag{48}$$

The potential difference $\Delta\phi = \phi_a - \phi_b = \phi_a - \phi(L,o)$ is given by

$$\Delta\phi = \frac{J_o}{\sigma}\left[\frac{cL}{w} + \frac{2w}{\pi^2}\sum_{n=1}^{\infty}\frac{1}{n^2}\tanh\frac{n\pi L}{w}\sin\frac{n\pi c}{w}\right] \quad . \qquad (49)$$

Equation (49) establishes the relation between the current density J_o and the applied potential difference $\Delta\phi$.

The x- and y-components of the current density J are given by

$$J_x = -\sigma\frac{\partial\phi}{\partial x}$$

$$= J_o\left[\frac{c}{w} + \frac{2}{\pi}\sum_{n=1}^{\infty}\frac{1}{n}\cdot\frac{\cosh\frac{n\pi x}{w}\cos\frac{n\pi y}{w}\sin\frac{n\pi c}{w}}{\cos\frac{n\pi L}{w}}\right] \qquad (50a)$$

$$J_y = -\sigma\frac{\partial\phi}{\partial y}$$

$$= J_o\left[-\frac{2}{\pi}\sum_{n=1}^{\infty}\frac{1}{n}\cdot\frac{\sinh\frac{n\pi x}{w}\sin\frac{n\pi y}{w}\sin\frac{n\pi c}{w}}{\cosh\frac{n\pi L}{w}}\right] \qquad (50b)$$

3.3. Numerical Results

Numerical calculations of J_x and J_y as functions of x and y have been carried out for various values of the geometrical parameters, c, w, and L. Plots of the contours of constant J_x and J_y (in units of J_o) are presented in Figures 29 and 30 for the case c = 0.2w and L = 4w. The channeling of the ion current into the Van der Waals gap is clearly evident. A plot of the contours of constant ϕ are shown in Figure 31. Deviations of the contours from straight lines appear as the Van der Waals gap is approached.

The total current in the x-direction I_x is given by

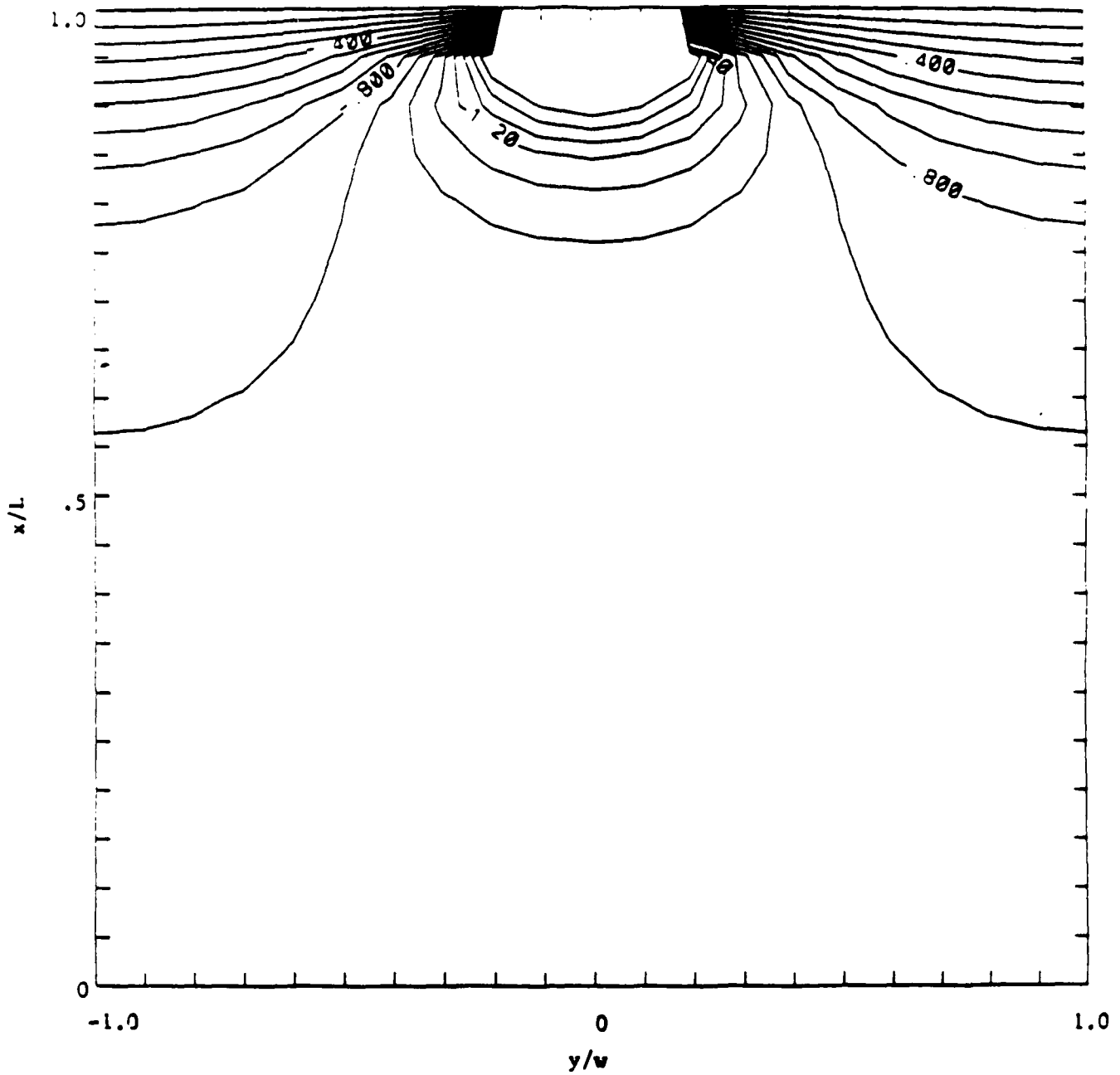

Figure 29. Contours of constant J_x.

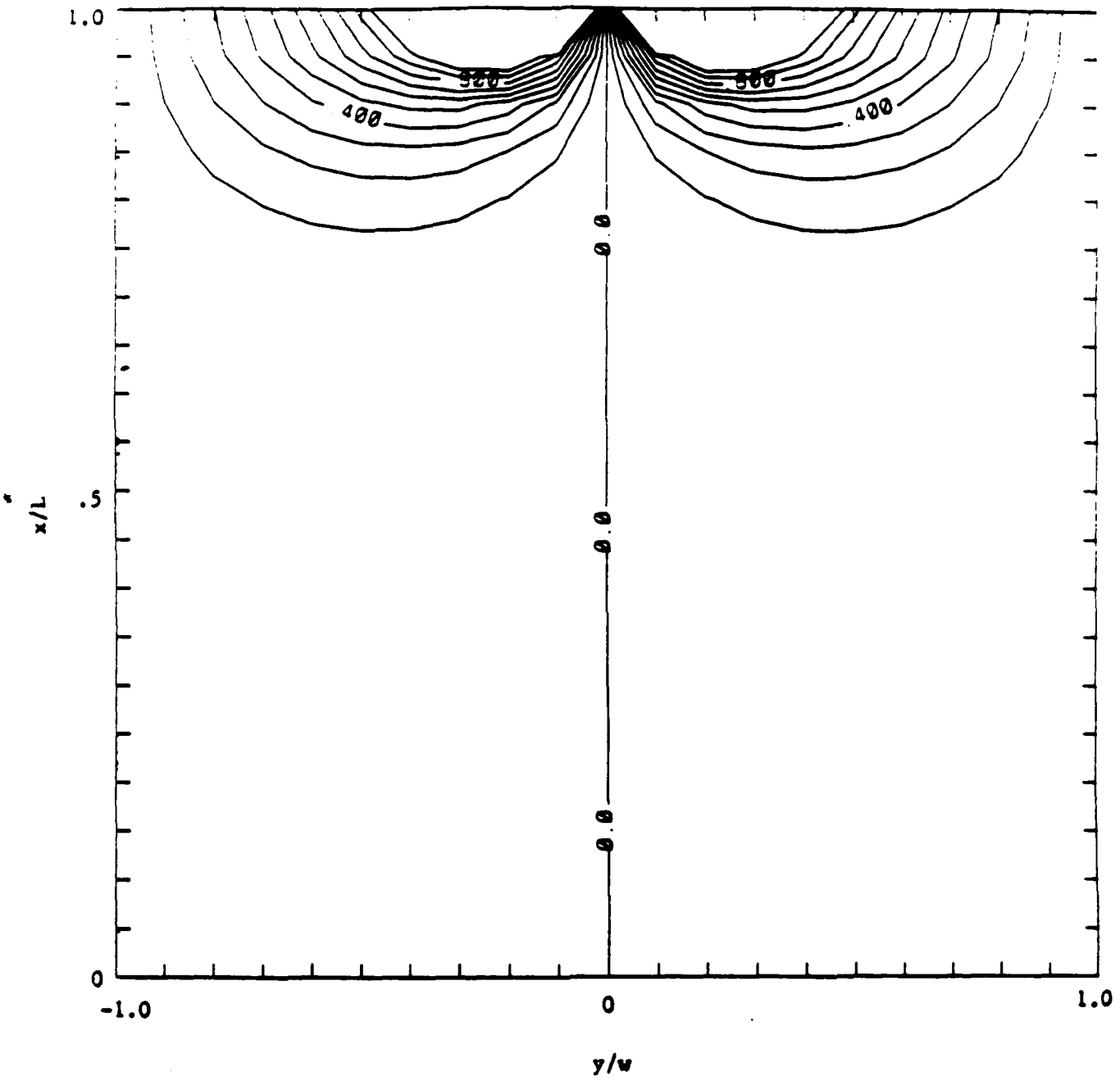

Figure 30. Contours of constant J_y.

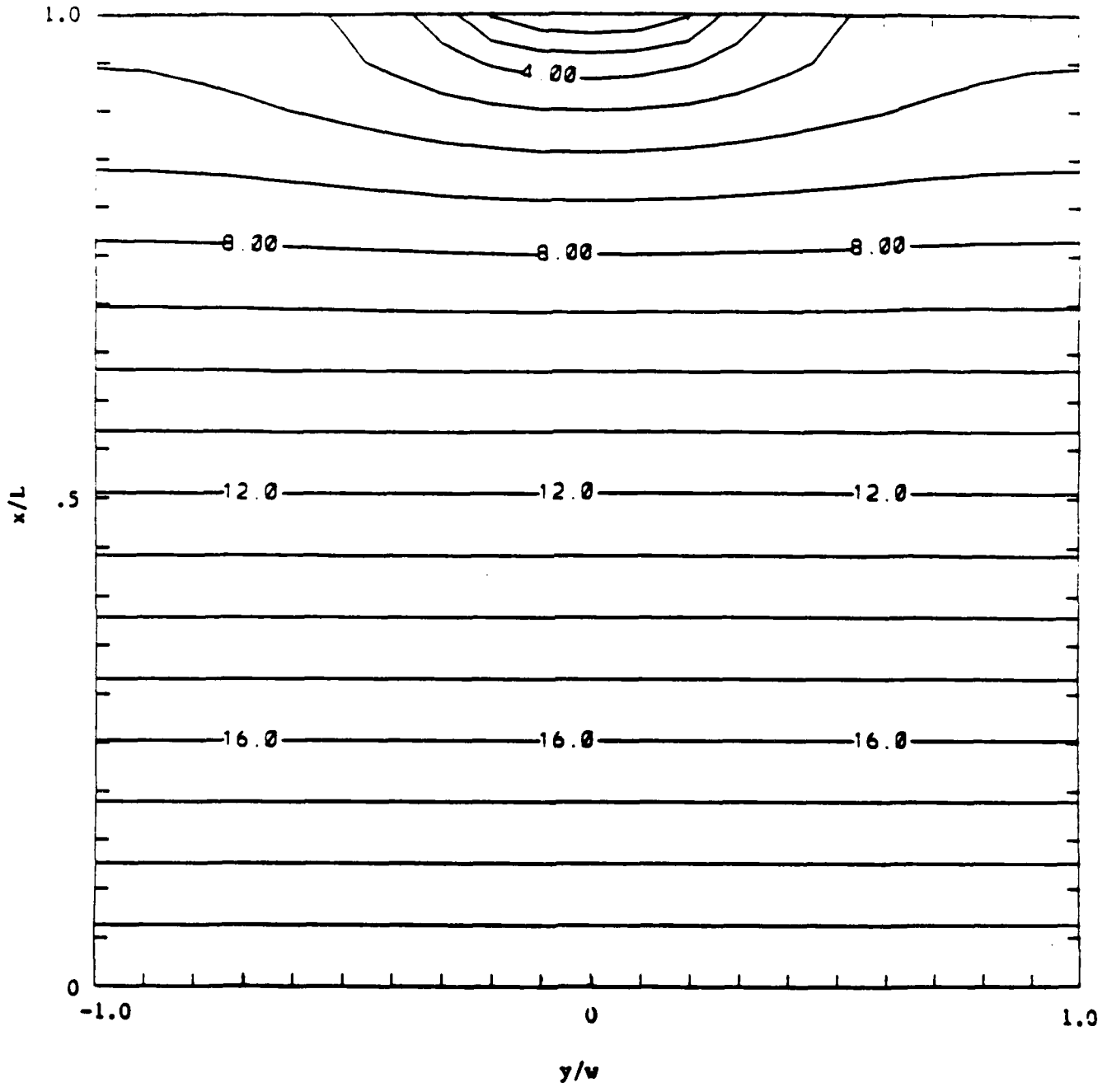

Figure 31. Contours of constant ϕ.

$$I_x = \int_{-w}^{w} J_x \, dy$$

$$= 2cJ_o \quad . \tag{51}$$

The effective resistance R of the lithium borate glass sample can be written as

$$R = \frac{\Delta\phi}{I_x} \quad . \tag{52}$$

Using Eqs. (50) and (51), we find that

$$R = \frac{1}{2c\sigma}\left[\frac{cL}{w} + \frac{2w}{\pi^2}\sum_{n=1}^{\infty}\frac{1}{n^2}\tanh\frac{n\pi L}{w}\sin\frac{n\pi c}{w}\right] \quad . \tag{53}$$

Numerical calculations have been made of R as a function of the ratio c/w for various values of the ratio L/2w, and the results are plotted in Figure 32. As the ratio c/w decreases below the value of 0.1, the effective resistance increases sharply. This effect may be of some importance in solid state batteries fabricated with thin films.

At the interface between the lithium borate glass and the InSe, there can be a potential barrier that the Li^+ ions must surmount in crossing the interface.

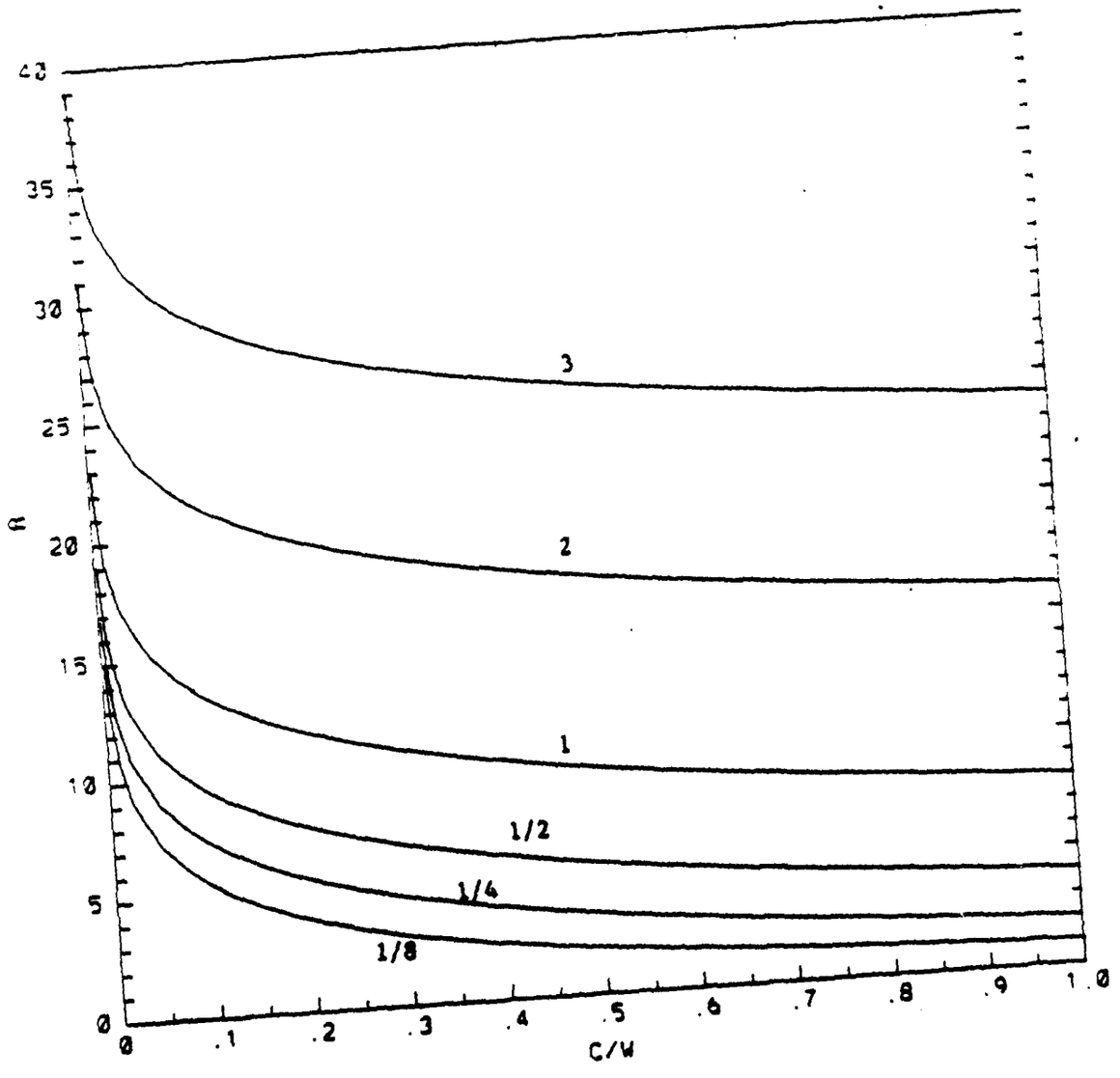

Figure 32. Effective resistance R versus c/w for various values of L/2w.

References

1. F. L. Galeener, R. A. Bario, E. Martinez and R. Elliott, Phys. Rev. Lett. 53, 2429 (1984).
2. P. J. Bray and G. O'Keefe, Phys. Chem. Glasses 4, 37 (1963).
3. T. V. Bril, Phillips Res. Rep. Suppl. 2 (1976).
4. M. Kbala, Thesis, Bordeaux (1984).
5. M. Balkanski, A. Ayyadi, P. Cadet, M. Jouanne, C. Julien, M. Massot, M. Scagliotti and A. Levasseur, Solid State Commun. 57, 41 (1986).
6. A. Ayyadi, Thesis Paris (1986).
7. Konijnendijk, Phillips Res. Rep. Suppl. (1975) n° 7.
8. M. Iron, M. Couzi, A. Levasseur, J. M. Reau and J. C. Brethous, J. of Solid State Chemistry 31, 285 299 (1980).
9. C. Wagner, International Committee of Electrochemical Thermodynamics and Kinetics, Proceed., 7th meeting, 955, Butterworths, London, 1956.
10. A. Levasseur, M. Kbala, J. C. Brethous, J. M. Reau, P. Hagen Muller and M. Couzi, Sol. State Commun. 32, 839 (1979).
11. L. Pauling, The Nature of the Chemical Bond, Cornell University Press, Ithaca, N.Y., 2nd ed., 1940.
12. F. Seitz, Rev. Mod. Phys. 26 (1954) 417.
13. A. B. Lidiard, Phys. Rev. 94 (1954) 29.
14. M. Balkanski, R. F. Wallis, I. Darianian and J. Deppe, Materials Science and Engineering, B1 (1988) 15-21.
15. E. Hazikaniotis, C. Julien and M. Balkanski, Mat. Res. Bull. 1984.
16. F. Herman and S. Skillman, Atomic Structure Calculations

(Prentice-Hall, Englewood Cliffs, 1963).

17. E. Doni, R. Girlanda, V. Grasso, A. Balzarotti, and M. Piacentini, Il Nuovo Cimento 51B, 154 (1979).

*U.S.Government Printing Office: 1989 — 648-056/04249